

MAPS: Preserving Vision-Language Representations via Module-Wise Proximity Scheduling for Better Vision-Language-Action Generalization

Chengyue Huang* Mellon M. Zhang* Robert Azarcon
 Glen Chou Zsolt Kira
 Georgia Institute of Technology
 {chuang475, meilongz, razarcon3, chou, zkira}@gatech.edu
[mapsvla.github.io](https://github.com/mapsvla)

Abstract

*Vision-Language-Action (VLA) models inherit strong priors from pretrained Vision-Language Models (VLMs), but naïve fine-tuning often disrupts these representations and harms generalization. Existing fixes – freezing modules or applying uniform regularization – either overconstrain adaptation or ignore the differing roles of VLA components. We present **MAPS (Module-Wise Proximity Scheduling)**, the first robust fine-tuning framework for VLAs. Through systematic analysis, we uncover an empirical order in which proximity constraints should be relaxed to balance stability and flexibility. MAPS linearly schedules this relaxation, enabling visual encoders to stay close to their pretrained priors while action-oriented language layers adapt more freely. MAPS introduces no additional parameters or data, and can be seamlessly integrated into existing VLAs. Across MiniVLA-VQ, MiniVLA-OFT, OpenVLA-OFT, and challenging benchmarks such as SimplerEnv, CALVIN, LIBERO, as well as real-world evaluations on the Franka Emika Panda platform, MAPS consistently boosts both in-distribution and out-of-distribution performance (up to +30%). Our findings highlight empirically guided proximity to pretrained VLMs as a simple yet powerful principle for preserving broad generalization in VLM-to-VLA transfer.*

1. Introduction

Vision-Language-Action (VLA) models have recently emerged as a unifying framework for robotic learning, enabling agents to perceive their environment, understand natural language instructions, and execute actions in an end-to-end manner [1–4]. However, the scarcity of large-scale robotics data makes it infeasible to train these models from scratch. As a result, most VLA systems initialize from pow-

erful vision-language models (VLMs) [5–7] pretrained on web-scale data, leveraging their rich visual and semantic priors before finetuning on robotics datasets to learn action policies. However, while this strategy has led to impressive task performance, it often comes at the cost of generalization – models degrade in performance when faced with novel tasks, objects, or environments [8, 9].

This loss of generalization arises from a fundamental mismatch between large-scale pretraining and the limited scope of robot-specific finetuning [1]. Robotics datasets are typically sparse and task-specific, and finetuning extensively on them induces spurious correlations and overfitting, which in turn causes catastrophic forgetting of spatial reasoning, world knowledge, and linguistic grounding. The core challenge in VLA training therefore lies in balancing the tradeoff between action adaptation and preservation of pretrained generalization. Excessive finetuning causes the model to drift too far from its pretrained initialization, diminishing robustness to distribution shifts [10]. Conversely, insufficient finetuning limits the model’s ability to align with the action space.

Several approaches attempt to balance adaptation and generalization. Freezing visual encoders preserves pretrained perception but limits adaptation to robotics-specific cues. Dual-encoder designs [9] maintain both frozen and trainable visual pathways, improving flexibility at the cost of doubled memory and compute. Weight interpolation techniques [8] gradually revert visual weights to their pretrained state while adapting the language backbone, but require multiple training stages. In these efforts, generalization often comes at the expense of higher computational and architectural complexity, with most methods emphasizing visual preservation while overlooking the role of semantic priors in language components.

Seeking a lightweight alternative to preserving pretrained knowledge, we begin by revisiting the common practice of model freezing. Through a systematic analysis

*Equal contribution.

of freezing different VLM components during action fine-tuning, we confirm a widely held but rarely quantified intuition: visual modules should remain strongly constrained. Early visual backbones such as DINOv2 [11] capture essential geometric and spatial priors for manipulation, whereas language-aligned modules like SigLIP [12] and deeper language layers benefit from greater flexibility to adapt task-specific semantics and action grounding. However, we also find that freezing itself introduces task-specific inductive biases, and certain freeze configurations fail to generalize across new domains and environments.

Instead of hard constraints from model freezing, soft regularization offers a more flexible and robust alternative with comparable efficiency [10, 13–16]. Projection-based selective tuning methods, such as selective projection decay [13], replace conventional weight decay with a projection operator that limits how far parameters drift from their pretrained values – enabling adaptive regularization across layers without added complexity. However, existing approaches typically use a single hyperparameter to enforce a uniform regularization strength, implicitly assuming all layers should deviate equally. We find this assumption ill-suited for VLA models, where different components encode distinct priors and vary in their sensitivity to fine-tuning. Some modules must stay near their pretrained state to preserve structural knowledge, while others require greater flexibility to adapt task-specific grounding.

This introduces a new tradeoff: naive freezing provides modularity but is brittle due to strong inductive bias, whereas robust finetuning relaxes this bias but sacrifices modularity. To bridge this tradeoff and successfully adapt the robust finetuning paradigm to the action domain, we propose **MAPS (Module-Wise Proximity Scheduling)**, a robust finetuning framework designed specifically for VLA models. MAPS extends traditional projection-based selective tuning [13] by modulating the *projection strength rate of change* hyperparameter across model components and training steps via a linear scheduler. This encourages more careful updates of the visual components to preserve pretrained geometric priors while allowing more explorative updates of the language components to quickly adapt to the action space. Importantly, this scheduling is implemented with no additional models, data, or parameters and integrates seamlessly with existing VLA architectures.

We validate MAPS across a wide range of VLA backbones, including MiniVLA-VQ [17, 18], MiniVLA-OFT, OpenVLA-OFT [19], etc. Experiments on a diverse set of evaluation benchmarks - SimplerEnv Bridge Data [20], CALVIN [21] (ABC→D), LIBERO [22] (train on LIBERO-90, test on Goal/Spatial/Object/Long), and real-world evaluations on a Franka Emika Panda robot consistently show that MAPS improves out-of-distribution (OOD) generalization while preserving pretrained structure and in-

distribution (ID) performance. These findings suggest that maintaining proximity to pretrained VLMs in a selective manner is a simple yet powerful principle that could guide future scaling and pre-training of VLA systems.

2. Related Works

Vision-Language-Action Models. Vision-Language-Action (VLA) models advance unified embodied intelligence by leveraging large pretrained foundation models [5–7] and their components [11, 12, 23]. Systems like RT-1, PaLM-E, and RT-2 [2, 3, 24] showed that grounding vision-language pretraining in experience enables cross-task transfer. Large frameworks such as Open-X Embodiment, OpenVLA, and π_0 [1, 4, 19, 25–27] scale data and architectures for generalization. Recent work improves action tokenization [18, 28–32], efficiency [17, 33, 34], and grounding/reasoning [35–41], while emerging work explores chain-of-thought reasoning for interpretable control [42–44]. Despite progress, most VLAs rely on fine-tuning that disrupts pretrained priors; MAPS instead preserves them via module-wise proximity scheduling for selective adaptation.

VLA Generalization. Improving generalization in VLA models focuses on preserving pretrained representations while adapting to new tasks. Data-oriented approaches reformulate robotic data for better VLM alignment (directional prediction [45] or textual trajectory conversion [46]) and co-train with action objectives [9, 28]. Training-oriented methods retain learned priors via weight interpolation [8], dual encoders [9], frozen cross-attention [47], embedding regularization [48], or action perturbation [49]. These add computational overhead, whereas MAPS constrains updates by module importance and proximity to pretrained weights, preserving priors and improving OOD generalization without extra data or parameters.

3. Background

3.1. Vision-Language-Action Models

A Vision-Language-Action (VLA) model [1, 3, 4, 15] seeks to learn a policy $\pi_\theta(a_t | o_t, x)$ that maps a multimodal observation o_t and a language instruction x to an action a_t in an embodied environment. Typically, the visual and language inputs are encoded by f_v and f_l separately, and fused by a multimodal transformer f_m to produce a policy embedding $z_t = f_m([f_v(o_t), f_l(x)])$. Action parameterization varies across families of VLAs: **continuous-action models** predict low-level control vectors directly and are trained to make their outputs closely match the expert’s actions, using objectives such as ℓ_1 regression [19], diffusion-based denoising [44], or flow matching [4]. In contrast, **discrete-action models** convert actions or short action segments into a finite set of tokens [1]. Modern VLAs build upon pre-

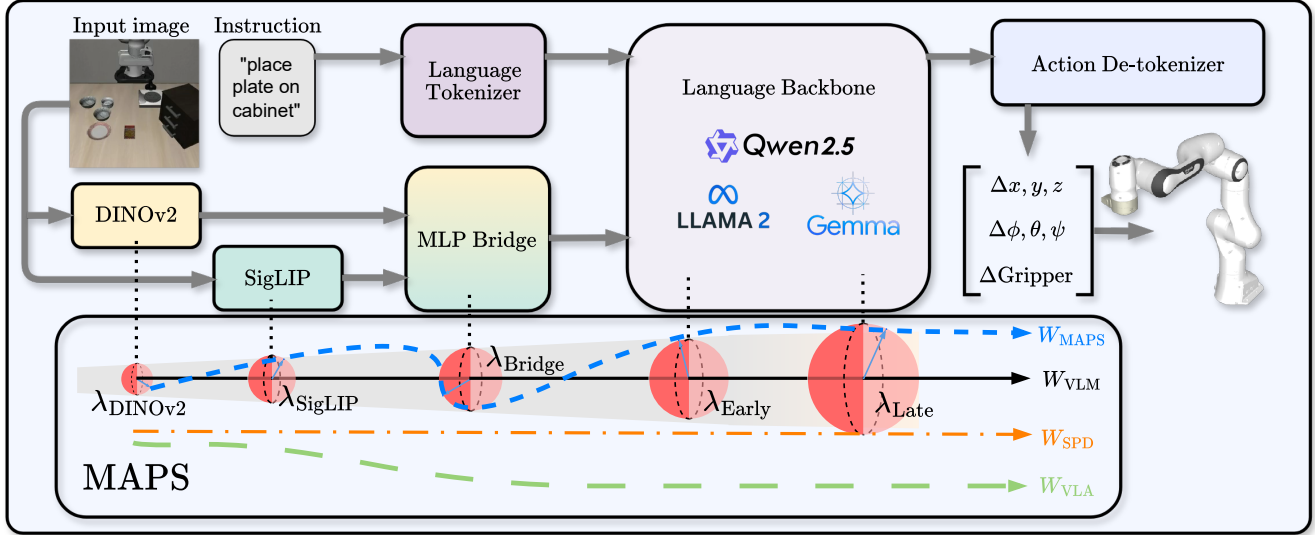


Figure 1. **Module-Wise Proximity Scheduling (MAPS)**. MAPS is applied on pretrained VLM components during the action finetuning stage. MAPS (blue dash line) enforces strong preservation on early vision layers while progressively relaxing constraints toward higher-level language layers. In contrast, vanilla finetuning (green dash line) distorts the VLM representation completely away from its pretrained weights (black solid line), and uniform SPD (orange dash/dot line) applies the same constraint everywhere.

trained vision-language backbones such as DINOv2 [11], SIGLIP [12], and LLAMA [7], using either a multi-modal transformer or a lightweight cross-attention “bridge” to fuse representations before an action head maps z_t into either continuous controls or discrete tokens. Models such as π_0 -Fast [29], and OpenVLA-OFT [19] follow this template but introduce small projection heads or adapters for rapid finetuning and deploying. During training on robot demonstrations, the model grounds linguistic semantics in action-conditioned representations that transfer across tasks, objects, and embodiments.

3.2. Robust Fine-Tuning

We revisit projection-based robust fine-tuning (RFT) methods [10, 13, 15, 50, 51] that constrain fine-tuning to remain close to the pretrained weights, enabling models to adapt to downstream tasks while preserving pretrain generalization. **From L2 regularization to projection.** Vanilla fine-tuning updates model parameters to minimize the task loss \mathcal{L} without constraining deviation from the pretrained model. This often leads to feature drift and catastrophic forgetting [10, 14, 15]. L2-SP [14] addresses this issue by penalizing the distance between the fine-tuned parameters θ_t and the pretrained initialization θ_0 with regularization strength λ_{reg} at each gradient iteration step t :

$$\mathcal{L}_{\text{L2-SP}} = \mathcal{L}(\theta_t) + \frac{\lambda_{\text{reg}}}{2} \|\theta_t - \theta_0\|_2^2. \quad (1)$$

Instead of regularizing $\|\theta_t\|_2$, L2-SP explicitly preserves proximity to the pretrained model. Building on this idea, TPGM [10] reformulates L2-SP by enforcing the model to

stay within a distance of γ from the pre-trained model:

$$\min \mathcal{L}(x, y; \theta_t), \quad \text{s.t.} \quad \|\theta_t - \theta_0\|_2 \leq \gamma. \quad (2)$$

To enforce this constraint during training, TPGM applies the *Projected Gradient Method* (PGM), projecting the updated weights back into an ℓ_2 ball with radius γ around θ_0 , where $\tilde{\theta}_t$ is the unconstrained updated weight:

$$\theta_t = \theta_0 + \frac{1}{\max\left(1, \frac{\|\tilde{\theta}_t - \theta_0\|_2}{\gamma}\right)} (\tilde{\theta}_t - \theta_0). \quad (3)$$

Selective Projection Decay (SPD). SPD [13] builds on the projection view of L2-SP and TPGM by determining whether and how much the unconstrained update $\tilde{\theta}_t$ should be projected back toward the pretrained weights θ_0 .

Step 1: When to project. Motivated by the derivative of \mathcal{L} w.r.t. λ_{reg} , i.e. $\frac{\partial \mathcal{L}(\theta_t)}{\partial \lambda_{\text{reg}}} = \frac{\partial \mathcal{L}(\theta_t)}{\partial \theta_t}^\top \frac{\partial \theta_t}{\partial \lambda_{\text{reg}}} = \alpha * -g_{t+1}^\top (\tilde{\theta}_t - \theta_0)$ where α is the learning rate and g is the gradient, SPD uses the sign of $c_t := -g_{t+1}^\top (\tilde{\theta}_t - \theta_0)$ as the selection condition, since it determines the direction of the hyper-update: if $c_t < 0$, gradient descent increases λ_{reg} and strengthens L2-SP regularization, whereas if $c_t > 0$, it decreases λ_{reg} and weakens the regularization. Thus, SPD triggers a projection step if $c_t < 0$; otherwise the update is left unchanged.

Step 2: How much to project. L2-SP’s optimization step after unconstrained update can be written as $\theta_t = \tilde{\theta}_t - \lambda_{\text{reg}} \alpha (\tilde{\theta}_t - \theta_0)$. Reformulating Eq. (3) as $\theta_t = \tilde{\theta}_t - \left(1 - \frac{\gamma}{\max\{\gamma, \|\tilde{\theta}_t - \theta_0\|_2\}}\right) * (\tilde{\theta}_t - \theta_0)$, L2-SP (regularization) and projection are equivalent if $\lambda_{\text{reg}} \alpha = \left(1 - \frac{\gamma}{\max\{\gamma, \|\tilde{\theta}_t - \theta_0\|_2\}}\right)$. SPD then defines a deviation ratio $r_t =$



Figure 2. Qualitative comparison of freezing configurations for LIBERO-90 task "put the bowl on the plate" (left to right: full fine-tuning (FFT), freeze VLM, freeze language, freeze vision). FFT fails most, targeting the cabinet instead of the bowl. Freezing VLM/language/vision preserves 2D localization of the bowl but impairs depth reasoning. When vision is frozen, the policy can grasp the bowl but fails to accurately place it on the plate.

$\frac{\max\{\gamma_t - \gamma_{t-1}\}}{\gamma_t}$ based on the current deviation radius (before regularization) $\gamma_t = \|\tilde{\theta}_t - \theta_0\|_2$ and the previous radius $\gamma_{t-1} = \|\theta_{t-1} - \theta_0\|_2$, and replace the learning rate α in L2-SP with the deviation ratio r_t . This makes the *new hyperparameter* λ tuning more intuitive, where $\lambda_{\text{reg}}\alpha = \lambda r_t$. Intuitively, with $\lambda = 1$, $\theta_t = \tilde{\theta}_t - \frac{\max\{0, \gamma_t - \gamma_{t-1}\}}{\gamma_t}(\tilde{\theta}_t - \theta_0) = \theta_0 + \frac{\gamma_{t-1}}{\max\{\gamma_{t-1}, \gamma_t\}} * (\tilde{\theta}_t - \theta_0)$, the regularization is equivalent to projecting the updated parameters onto a ball with radius equal to the previous deviation whenever the current deviation exceeds that value. Now, a single hyperparameter λ replaces the conventional weight decay and controls how aggressively the constraint radius expands or contracts during training. When $\lambda = 0$, SPD reduces to full fine-tuning with no projection; $0 < \lambda < 1$ allows the radius to expand, enabling flexible adaptation; $\lambda = 1$ keeps the deviation from the pretrained model fixed; and $\lambda > 1$ contracts the radius, pulling parameters back toward θ_0 . Despite being a single scalar, λ enables dynamic and layer-specific projection across optimization steps.

4. Method

4.1. Catastrophic Forgetting in VLAs

VLA models are well known to struggle with zero-shot generalization across new tasks, environments, and instructions. Prior work traces this largely to catastrophic forgetting during action finetuning. ReVLA [8] attributes the issue to collapse in the DINOv2 [11] encoder, where depth estimation degrades into low-detail, spatially uniform maps – losing the rich geometry preserved in the pretrained DINOv2 features of PrismaticVLM [52]. [48] similarly find that fine-tuned VLAs attend to irrelevant regions under OOD conditions, with t-SNE analyses revealing compressed, degenerate feature spaces. [9] further observe over-sensitivity to background variation and instruction phrasing, suggesting overfitting to language form rather than meaning. Collectively, these studies identify action finetuning as the primary source of generalization failure, motivating efforts to preserve VLM representations during adaptation.

Freezing parts of a pretrained VLM is a simple yet ef-

fective way to preserve learned representations, preventing weights from drifting in suboptimal directions during fine-tuning. Recent works have refined this idea in various ways: [9] freeze the vision encoder and train a separate copy, [48] regularize against a frozen teacher, and ReVLA [8] interpolates vision-encoder weights between pretrained and adapted models while tuning the language backbone. While these strategies improve generalization, they often incur extra computation and supervision. Motivated by this line of work, we investigate how far simple freezing alone can bridge the generalization gap between VLMs and VLAs.

4.2. How good is model freezing?

To study the impact of model freezing, we decompose the VLA architecture into four components – DINOv2, SigLIP, early language layers, and late language layers – and systematically evaluate different freezing configurations on both ID and OOD settings. We focus on the OpenVLA [1] family, which integrates a joint DINOv2–SigLIP visual encoder. This modular design allows precise control over which capabilities are retained during adaptation: DINOv2 contributes depth perception and geometric priors, while SigLIP provides strong vision–language alignment. To ensure coverage across model scales and benchmarks, we conduct experiments with VLA-Adapter [53] on LIBERO and MiniVLA-OFT [17] on SimplerEnv BridgeV2 (see Sec. 5 for experimental details).

Our results (Tables 1 and 2) reveal several key insights into the efficacy of freezing:

1. **Language adaptation is essential.** Freezing the language backbone severely limits adaptation to the action space, yielding near-zero performance on SimplerEnv and up to a 60% drop on LIBERO.
2. **Freezing the vision encoder generally improves performance.** On SimplerEnv, ID accuracy increases by 7–17% and OOD by 7–25%; on LIBERO, gains are smaller but consistent (around 5% ID). In Fig. 2, freezing vision components allows the robot arm to grasp the bowl, whereas all other configurations struggle.
3. **Late language layers drive task performance.** Fine-tuning late language layers while freezing early ones boosts OOD generalization by 1–3%, aligning with their direct role in producing action outputs.
4. **Preserving DINOv2 matters more than SigLIP.** Freezing DINOv2 yields roughly 5% higher OOD performance than freezing SigLIP, underscoring the importance of maintaining strong geometric priors.
5. **Freezing effects are not universally consistent.** Freezing demonstrates improvements over full fine-tuning. Yet, some configurations (ex. freeze early language) improve one benchmark but harm another, indicating that freezing introduces task-dependent inductive biases.

Overall, our findings suggest a hierarchy of importance

Table 1. Comparison of freezing or robust fine-tuning (RFT) different parts of VLA on SimplerEnv’s ID and OOD tasks (details in Sec. 5.1). Early L and Last L denote early and the last language layers. ❄️ and 🔥 represent freeze and full fine-tune.

Modules				ID					OOD			
DINOV2	SigLIP	Early L	Last L	T1: Spoon	T2: Carrot	T3: Stack	T4: Eggplant	Avg. ID	Visual	Novel Object	Novel Category	Avg. OOD
MiniVLA-OFT [†]				22.0	30.0	0.0	2.0	13.5	12.7	2.0	12.0	8.9
❄️	❄️	🔥	🔥	22.0	24.0	0.0	34.0	20.0	20.0	13.3	10.7	15.0
🔥	🔥	❄️	❄️	0.0	0.0	0.0	0.0	0.0	1.3	0.0	2.7	1.2
❄️	❄️	🔥	🔥	0.0	0.0	0.0	0.0	0.0	0.0	0.0	0.0	0.0
❄️	🔥	❄️	🔥	42.0	32.0	6.0	42.0	30.5	32.7	51.3	11.3	33.6
🔥	❄️	🔥	🔥	12.0	10.0	12.0	90.0	31.0	29.3	35.3	22.7	29.7
🔥	🔥	❄️	🔥	0.0	0.0	0.0	0.0	0.0	4.0	0.7	2.0	2.2
RFT				4.0	8.0	0.0	94.0	26.5	6.7	20.0	14.0	13.6

Table 2. Comparison of freezing different parts of VLA on LIBERO. Early L and Last L denote early and the last language layers. ❄️ and 🔥 represent freeze and full fine-tune.

Modules				ID	OOD				
DINOV2	SigLIP	Early L	Last L	LIBERO-90	-Spatial	-Object	-Goal	-Long	Avg. OOD
VLA-Adapter [†]				83.0	2.0	5.0	1.0	2.0	2.5
❄️	❄️	🔥	🔥	92.0	0.0	3.0	0.0	6.0	2.3
🔥	🔥	❄️	❄️	29.0	1.0	4.0	1.0	0.0	1.5
❄️	❄️	🔥	🔥	19.0	0.0	0.0	1.0	0.0	0.3
❄️	🔥	❄️	🔥	89.0	0.0	6.0	0.0	6.0	3.0
🔥	❄️	🔥	🔥	73.0	1.0	0.0	0.0	3.0	1.0
🔥	🔥	❄️	🔥	91.0	0.0	4.0	6.0	8.0	4.5
RFT				88.0	1.0	2.0	0.0	6.0	2.3

among modules:

DINOV2 > SigLIP > Early language > Late language

Yet, **freezing alone is not a reliable path to generalization**. While it allows selective preservation of pretrained knowledge, it also imposes strong biases that can degrade performance in unseen settings. A more robust alternative lies in soft regularization, where finetuning is guided rather than restricted.

4.3. From hard constraints to soft constraints

The robust finetuning (RFT) literature (see Sec. 3.2) offers a natural foundation for our goal of constraining weight updates while preserving pretrained representations. In principle, RFT lowers task loss while keeping parameter drift minimal. While the intuition fits seamlessly with our goals, we find that naively applying RFT directly on the action finetuning offers only modest improvements over the baseline in both SimplerEnv (Tab. 1) and LIBERO (Tab. 2). This is because RFT techniques impose a single hyperparameter constraint across the entire model, meaning that layers either constrict closer towards or expand away from the pretrained weights at a uniform rate. As shown at the bottom of Fig. 3, this results in all components of the VLM diverging equal amounts from their pretrained representations. As we observed from Sec. 4.2, however, different components should evolve at different rates – some should be allowed more flexibility to adapt to the action space, whereas others should be constrained to preserve their pretrained priors.

4.4. Module-Wise Proximity Scheduling

Our preliminary studies highlights a key tradeoff: model freezing offers high modularity at the cost of heavy inductive bias, RFT offers lighter inductive bias but has no modularity. To bridge the two paradigms and successfully adapt robust finetuning for the action domain, we introduce a new framework of RFT methods specifically tailored for VLA models, known as **Module-Wise Proximity Scheduling (MAPS)**.

MAPS assigns distinct proximity schedules to different components of the base VLM, enabling strong preservation where pretrained structure is crucial (e.g., early vision and early language layers) while allowing more aggressive adaptation where grounding to actions is most beneficial (e.g., higher-level language layers and the action head). In other words, MAPS is designed to *learn when to preserve and when to adapt*, avoiding the rigidity of full freezing and the instability of uniform finetuning.

Concretely, MAPS modifies SPD by replacing its *global* proximity hyperparameter λ with a *layer-wise*, architecture-aware schedule. Let $\mathcal{L} = (\ell_1, \dots, \ell_{|\mathcal{L}|})$ denote the ordered stack of model submodules (DINOV2 \rightarrow SigLIP \rightarrow BRIDGE \rightarrow LANGUAGE). For each layer index k , MAPS assigns a proximity weight

$$\lambda_k = \lambda_{\max} \left(1 - \frac{k-1}{|\mathcal{L}|-1} \right),$$

yielding a linear decay from $\lambda_1 = \lambda_{\max}$ for early visual layers to $\lambda_{|\mathcal{L}|} = 0$ for language layers. In addition, MAPS assigns $\lambda_k = 0$ for all modules that are initialized from scratch, such as the action head, proprioceptive-state projector, and other non-pretrained components. Since these modules have no pretrained parameters θ_0 to preserve, MAPS simply performs full fine-tuning on them.

During optimization, let θ denote the parameters of the current layer, θ_0 their pretrained initialization, and g_t the gradient at iteration t . MAPS first computes an unconstrained step $\tilde{\theta}_t$, after which it evaluates the gradient-displacement correlation

$$c_t := -g_t^\top (\theta_{t-1} - \theta_0).$$

Whenever $c_t < 0$, indicating that the update direction is inconsistent with preserving pretrained structure, MAPS applies a projection toward θ_0 with *layer-specific* strength:

$$\theta_t \leftarrow \tilde{\theta}_t - \lambda_k r_t (\tilde{\theta}_t - \theta_0),$$

where r_t is the SPD deviation ratio (see Sec. 3.2).

Unlike SPD, which uses a single global constraint and therefore cannot differentiate between layers with distinct gradient scales or semantic roles, MAPS explicitly encodes architectural structure: visual layers remain strongly anchored to pretrained perceptual representations, while deeper language layers are allowed to adapt more flexibly to task-level semantics. This is highlighted in Fig. 3, where DINOv2 weights diverge least, followed by SigLIP weights, and finally language weights adapt most. As shown in Sec. 6, the linear schedule outperforms constant and cosine alternatives, underscoring the importance of structured, layer-wise proximity control.

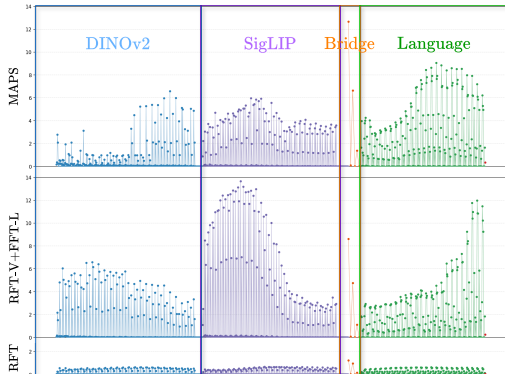


Figure 3. We calculate the ℓ_2 distance between fine-tuned and pre-trained weights. MAPS produces a smooth, module-aware decay in deviation from pretrained initialization (top). Applying robust finetuning only to the vision stack and full finetuning on language (RFT-V+FFT-L) constrains DINOv2 heavily but leaves SigLIP and language relatively unconstrained (middle). Uniform λ (RFT) constrains all layers equally (bottom).

MAPS is lightweight and plug-and-play: it introduces no additional parameters, requires no auxiliary networks or extra data, and can be applied to existing VLA architectures without modification. By directly encoding the empirical hierarchy revealed in our preliminary studies, MAPS strikes an effective balance between retaining essential pretrained priors and adapting to new action domains.

5. Experiments

We evaluate MAPS through three guiding questions. **(RQ1)** How well does it generalize across ID and OOD tasks? To test this, we use three diverse benchmarks – SimplerEnv [20] (Sec. 5.1), CALVIN [21] (Sec. 5.2), and LIBERO

[22] (Sec. 5.3) – that span semantic, environmental, and visual shifts, providing a comprehensive measure of robustness. **(RQ2)** Are MAPS’ gains consistent across architectures? We evaluate four state-of-the-art VLA backbones – MiniVLA-VQ, MiniVLA-OFT, VLA-Adapter, and OpenVLA-OFT – to test architecture-agnostic benefits. **(RQ3)** Does the robustness afforded by MAPS transfer to real-world deployment? We assess real-world transfer by deploying MAPS on a Franka Emika Panda manipulator (Sec. 5.4). Importantly, across all benchmarks, *we evaluate MAPS by fine-tuning the base VLM weights directly*. In other words, we initialize each VLA backbone from its pretrained VLM and train it from scratch using MAPS.

Backbones. Because MAPS does not rely on architecture-specific hyperparameters or task-specific loss modifications, it can be dropped into models with any visual encoder, language model, or action tokenization strategy. To demonstrate this flexibility, we instantiate MAPS across four widely used VLA backbones: MiniVLA-VQ [17], MiniVLA-OFT, OpenVLA-OFT [19], and VLA-Adapter [53]. MiniVLA pairs a DINOv2-SigLIP visual stack with a Qwen2.5-0.5B [6] language model; the VQ variant replaces the typical uniform discretized action bins with a vector-quantized VAE [18], enabling multi-step action chunking from a single forward pass. OpenVLA-OFT instead uses a LLaMA-2 7B [7] backbone and a parallel decoding head that directly regresses continuous actions via an ℓ_1 loss, fully avoiding discretization. By implementing this OFT-style action head on the MiniVLA backbone, we also create a lightweight MiniVLA-OFT variant, allowing us to test our method with both small and large LMs while holding other components fixed. Finally, VLA-Adapter introduces a lightweight action head with Bridge Attention, enabling efficient and low-cost VLA training.

5.1. Performance on SimplerEnv

Experimental setting. SimplerEnv is a lightweight simulation benchmark for efficient robotic manipulation evaluation. Because its tasks are originally text-only, we follow [55] to add visual observations and align it with the VLA setting. For ID evaluation, we use the standard WidowX BridgeData V2 Visual Matching setup and report performance on four tasks: spoon on towel, carrot on plate, stack cube, and put eggplant in basket. For OOD evaluation, we adopt the extended suite from [55], which includes: (1) Visual Generalization, placing three ID tasks in unseen environments; (2) Novel Object, introducing new instances from known categories; and (3) Novel Category, involving entirely new object types. All VLA backbones are pretrained from scratch on the ID tasks, and we report success rates on both ID and OOD splits (Table 3). We also include prior VLA baselines, though these benefit from large-scale pretraining before fine-tuning on SimplerEnv.

Table 3. **SimplerEnv Results.** ID includes 4 tasks following SimplerEnv-Bridge setup. OOD evaluation suites include Visual, Novel Object, and Novel Category. * model checkpoints borrowed from original papers. † models pretrained from scratch on SimplerEnv.

Model	ID					OOD			
	T1: Spoon	T2: Carrot	T3: Stack	T4: Eggplant	Avg. ID	Visual	Novel Object	Novel Category	Avg. OOD
RT-1-X [2]	4.2	0.0	0.0	0.0	1.1	0.0	4.0	6.1	3.4
Octo [54, 55]	12.5	41.7	15.8	0.0	17.5	12.6	10.8	8.4	10.6
π_0 [4]	52.5	87.9	83.8	52.5	69.2	71.4	30.2	21.0	40.9
MiniVLA-VQ † [17]	52.0	24.0	42.0	58.0	44.0	37.3	34.0	27.3	32.9
+MAPS (Ours)	44.0	30.0	76.0	20.0	42.5	48.0	26.0	29.3	34.4
Δ	-8.0	+6.0	+34.0	-38.0	-1.5	+10.7	-8.0	+2.0	+1.5
MiniVLA-OFT†	22.0	30.0	0.0	2.0	13.5	12.7	2.0	12.0	8.9
+MAPS (Ours)	34.0	38.0	0.0	48.0	30.0	32.0	48.7	26.7	35.8
Δ	+12.0	+8.0	+0.0	+46.0	+16.5	+19.3	+46.7	+14.7	+26.9
OpenVLA-OFT† [19]	16.0	18.0	0.0	58.0	23.0	16.0	9.3	0.7	8.7
+MAPS (Ours)	2.0	16.0	0.0	74.0	23.0	18.7	20.0	12.7	17.1
Δ	-14.0	-2.0	+0.0	+16.0	+0.0	+2.7	+10.7	+12.0	+8.4

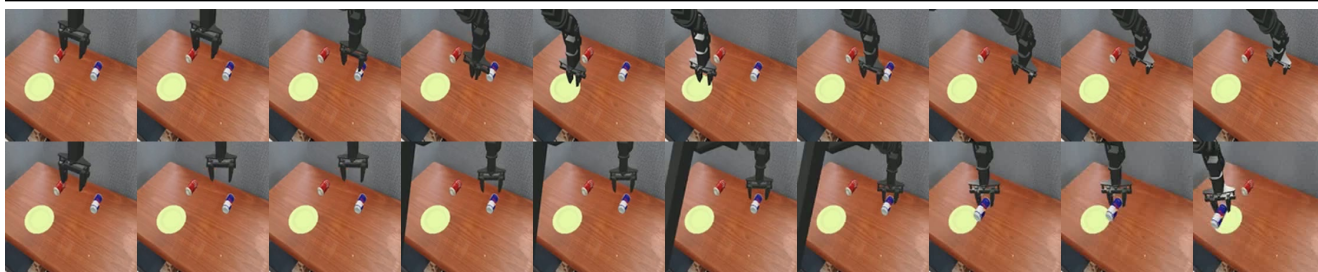


Figure 4. SimplerEnv qualitative example (new object: Red Bull can). Top: Full fine-tuning fails to complete the task. Bottom: MAPS successfully places the can on the plate.

Evaluation results. On MiniVLA-OFT, MAPS matches the ID performance of Vanilla finetuning, but demonstrates 10-20% improvement on OOD generalization. Notably, despite a substantially smaller pretraining corpora of just the BridgeData V2 Visual Matching tasks, MAPS matches and even surpasses the OOD generalizability of much larger and much more extensively pretrained baselines such as RT-1-X, Octo and π_0 . On MiniVLA-VQ, MAPS maintains similar ID performance and offers a moderate increase in OOD performance. On OpenVLA-OFT, MAPS maintains similar ID performance and improves average OOD by 8.4%. Again, this suggests that MAPS scales effectively across a variety of backbone sizes and architectures (RQ2).

5.2. Performance on CALVIN

Experimental setting. CALVIN features long-horizon tabletop manipulation tasks in a real-to-sim setting, partitioned into the A, B, C, and D splits that increasingly withhold task-environment combinations. We follow the standard ABC→D protocol: models are trained on splits A-C and evaluated OOD on split D. Evaluation uses CALVIN’s long-horizon, multi-task language control setup, where agents must complete sequences of five instructions; each new instruction is provided only after the previous one is completed, with success defined by reaching the instruction’s goal state. The benchmark reports two metrics: *tasks*

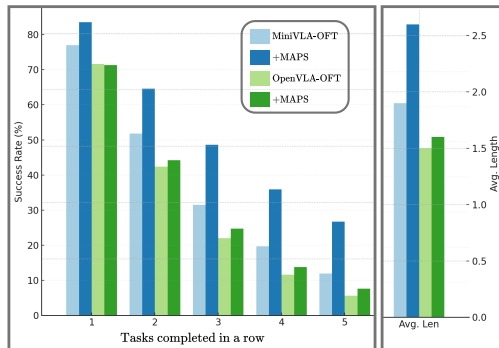


Figure 5. **CALVIN Results.** MAPS improves success rates across all action horizons (25% for MiniVLA-OFT and 3% for OpenVLA-OFT) and average length (+0.7 for MiniVLA-OFT and +0.1 for OpenVLA-OFT).

completed in a row, the success rate for completing exactly k consecutive tasks ($k = 1-5$), and *average length* (*avg. len*), the mean number of tasks completed per five-instruction sequence across all episodes.

Evaluation results. As shown in Fig. 5, MAPS leads to a +0.7 gain in average sequence length and consistently improves success rates across all task horizons on MiniVLA-OFT. The largest gains are observed for longer horizons: MAPS improves the success rate of completing 2-, 3-, 4-, and 5-task sequences by roughly 15% each, while the 1-task

success rate increases by 7%. MAPS demonstrates modest improvements over OpenVLA-OFT, boosting success rates by 2% across task horizons. Notably, MAPS demonstrates larger gains on stronger baselines, suggesting that it complements rather than replaces existing capabilities, and scales effectively with model quality (RQ2).

5.3. Performance on LIBERO

Table 4. **LIBERO Results.** * models borrowed from [17]. † models pretrained from scratch on LIBERO-90. ‡ models finetuned on LIBERO-90.

Model	ID (%)	OOD (%)				
	LIBERO-90	-Spatial	-Object	-Goal	-Long	Avg. OOD
OpenVLA	61.4	-	-	-	-	-
miniVLA*	62.0	0.0	0.0	0.0	1.0	0.25
miniVLA-VQ*	77.0	0.0	0.0	3.0	1.0	1.0
miniVLA-hist.*	82.0	0.0	1.0	2.0	7.0	2.5
miniVLA-wrist*	82.1	0.0	0.0	0.0	0.0	0.0
SpatialVLA‡	46.2	0.0	0.0	0.67	1.33	0.5
MiniVLA-VQ†	79.0	0.0	0.0	0.0	0.0	0.0
+MAPS (Ours)	82.0	0.0	1.0	8.0	10.0	4.75
Δ	+3.0	+0.0	+1.0	+8.0	+10.0	+4.75
MiniVLA-OFT†	91.0	0.0	8.0	7.0	4.0	4.75
+MAPS (Ours)	91.0	6.0	14.0	0.0	8.0	7.0
Δ	+0.0	+6.0	+6.0	-7.0	+4.0	+2.25
VLA-Adapter†	83.0	2.0	5.0	1.0	2.0	2.5
+MAPS (Ours)	88.0	0.0	7.0	6.0	6.0	4.75
Δ	+5.0	-2.0	+2.0	+5.0	+4.0	+2.25
OpenVLA-OFT†	92.0	3.0	9.0	3.0	5.0	5.0
+MAPS (Ours)	90.0	0.0	11.0	1.0	10.0	5.5
Δ	-2.0	-3.0	+2.0	-2.0	+5.0	+0.5

Experimental setting. The LIBERO benchmark consists of procedurally generated household manipulation tasks designed to evaluate generalization across task configurations, object appearances, and spatial layouts. It includes several predefined splits – LIBERO-90, LIBERO-Long, LIBERO-Goal, LIBERO-Spatial, and LIBERO-Object – each targeting a specific type of generalization, such as task diversity, long-horizon planning, unseen goals, spatial rearrangements, or novel objects. Agents are evaluated in a reset-free setting and must complete multi-step tasks from natural language instructions.

Previous works often rely on large-scale external pre-training – such as on Open X Embodiment – followed by fine-tuning separate model variants for each LIBERO split, and reporting results using these tailored models. In contrast, **our approach uses no external pretraining whatsoever.** Instead, we follow the more challenging protocol of [53]: we pre-train solely on the LIBERO-90 subset, and evaluate both ID performance on LIBERO-90 and OOD generalization on LIBERO-Spatial, LIBERO-Object, LIBERO-Goal, and LIBERO-Long. We report the success rates using 10 trials per task in Table 4.

Evaluation results. MAPS delivers consistent improvements in OOD performance across all four model backbones, yielding an average gain of 1–5%. Notably, the

base MiniVLA model shows no inherent OOD generalization capability; however, with MAPS, its performance increases by 8% on LIBERO-Goal and 10% on LIBERO-Long. For MiniVLA-OFT, MAPS enhances generalization on LIBERO-Spatial and LIBERO-Object by 6%. Similarly, MAPS improves the VLA-Adapter’s performance on LIBERO-Goal and LIBERO-Long by 5% and OpenVLA-OFT’s performance on LIBERO-Long by 5%. Beyond OOD gains, MAPS also provides moderate improvements on ID tasks, boosting MiniVLA-VQ performance by 3% and VLA-Adapter by 5%. This suggests that MAPS’ gains are indeed consistent across architectures and generalize well to different action tokenization schemes (RQ2). These results, in conjunction with results on the other benchmarks, also suggest that MAPS generalizes effectively across diverse ID and OOD tasks (RQ1).

5.4. Performance on Franka Emika Panda

Experimental setting. We conduct real-world tabletop manipulation experiments using a single Franka Emika Panda robotic arm. We form a pretraining corpora of 600 demonstrations across 4 different ID training tasks following [56], which are:

1. Coke ID: grab the coke can and lift it up,
2. Blocks ID: stack the blue block on the green block,
3. Cups ID: stack the orange cup onto the green cup,
4. Laptop ID: close the laptop lid fully.

We train MiniVLA-OFT (directly updating the VLM weights) using our self-collected demonstration dataset with both vanilla finetuning and MAPS.

To assess generalization, we evaluate the trained policies on the 4 ID tasks as well as on 4 corresponding OOD variants. The OOD tasks introduce controlled distribution shifts while preserving the underlying manipulation objectives. Specifically:

1. Coke OOD: coke can is replaced with red bull can;
2. Blocks OOD: blue block is elevated by placing an additional block underneath it;
3. Cups OOD: orange and green cups are replaced with yellow and blue cups, respectively;
4. Laptop OOD: Alienware laptop is replaced with a MacBook.

Overall, we design the OOD tasks to systematically probe performance under diverse distribution shifts. Coke OOD introduces novel instruction, class (Red Bull can), object geometry, and color. Blocks OOD tests novel elevation (elevated blue block). Cups OOD tests novel instruction and color. Laptop OOD tests novel class, color, object geometry, and altered physics (joint stiffness). For each task, including both ID and OOD variants, we conduct 10 evaluation trials using two object-location configurations, with 5 trials per configuration. All evaluations are executed in the real-world setup using the same Franka system as in training

Table 5. **Franka Results.**

Model	ID					OOD				
	T1: Coke	T2: Block	T3: Cup	T4: Laptop	Avg. ID	T1: Coke	T2: Block	T3: Cup	T4: Laptop	Avg. OOD
MiniVLA-OFT [†]	30.0	30.0	0.0	100.0	40.0	50.0	20.0	0.0	30.0	22.5
+MAPS (<i>Ours</i>)	50.0	70.0	80.0	90.0	72.5	100.0	30.0	20.0	60.0	52.5
Δ	+20.0	+40.0	+80.0	-10.0	+32.5	+50.0	+10.0	+20.0	+30.0	+30.0

with a max limit of 500 timesteps. We present our quantitative results below. We also provide qualitative results, rollout visualizations, setup details, and an in-depth results discussion along with observed success and failure modes in Appendix Sec. 8.

Evaluation results. Table 5 presents the success rates for each task together with the overall average performance. MAPS yields substantial gains over MiniVLA-OFT on both ID and OOD tasks. On the ID tasks, MAPS raises average performance from 40.0% to 72.5%, demonstrating much stronger policy learning from limited demonstrations. MAPS also improves generalization under distribution shift, boosting average OOD success from 22.5% to 52.5%. Overall, MAPS consistently enhances robustness and task success across diverse manipulation scenarios, showing clear benefits for real-world policy training.

Fine-grained task analysis. Beyond reporting aggregate success rates, we also provide a more fine-grained analysis of MAPS in Fig. 6, differentiating non-trivial competency on intermediate steps. To this end, we decompose the multi-step Task 2: Block (Fig. 6 Top) and Task 3: Cup (Fig. 6 Bottom Right) into a sequence of subtasks: (1) locating object 1, (2) picking up object 1, (3) locating object 2, and (4) stacking object 1 on object 2. We record the success rates on each of these subtasks for a closer look at potential failure modes. For Task 2 specifically, we additionally introduce a "Hard" setting (see Appendix Sec. 8.1) in which the block configuration is made more challenging than the "Easy" setting reported in Table 6. In the Hard ID variant, the distance between the two blocks is increased, while in the Hard OOD variant, object 1 (the blue block) is replaced with a red block. Finally, we also track how many attempts each method needs to complete a rollout (Fig. 6 Bottom Left). For Task 1 and Task 4, which have no intermediate subtasks, this value is simply the number of tries until the task succeeds. For Task 2 and Task 3, which include multiple subtasks, we record attempts only for the grasping subtask, as it is the only stage where the policy can retry.

MAPS’s fine-grained evaluations show that its biggest advantages come from more reliable grasps, more accurate intermediate localization, and more stable multi-step execution across all object categories. In Blocks ID (Easy), MAPS strengthens later-stage performance, improving second-block localization (80% vs. 50%), more than doubling final placements (70% vs. 30%), and reducing grasp attempts (1.13 vs. 1.56). Similar gains appear

in Blocks OOD (Easy), boosting first-block grasping (60% vs. 30%), second-block localization (60% vs. 20%), and final placement (30% vs. 20%), indicating robustness to modest distribution shift. Under Hard settings, both models degrade, but MAPS still reduces repeated grasps on Blocks ID (1.4 vs. 4.2). In Blocks OOD (Hard), where object 1 is fully OOD, the baseline fails entirely while MAPS maintains non-trivial competence – 70% first-block localization, 20% initial grasps, and 10% second-block localization – showing resilience to combined geometric and appearance shifts. For cup stacking, MAPS substantially improves every sub-stage: grasp-first success (80% vs. 20%), second-object localization (80% vs. 10%), final stacking (80% vs. 0%), and grasp attempts (1.0 vs. 1.5) in Cups ID; and in Cups OOD, the baseline fails beyond initial localization while MAPS successfully grasps, relocates, and stacks (2 trials each), demonstrating clear generalization. For laptop closing, both models locate and push the lid, but MAPS excels on the harder metric of fully closing: in Laptop ID it remains near-perfect (90% vs. 100%) with fewer attempts (1.22 vs. 1.75), and in Laptop OOD it doubles the fully closed rate (60% vs. 30%), showing better control accuracy under appearance change. For coke can lifting, MAPS improves success in both ID (50% vs. 30%) and OOD (100% vs. 50%), with slightly fewer attempts in ID (3.20 vs. 3.67); its perfect OOD score reflects strong appearance invariance. Overall, MAPS not only boosts final task success but consistently improves intermediate sub-task reliability across both ID and OOD conditions.

6. Ablation Studies

We design our ablation studies to rigorously evaluate our design choices and compare against prior approaches. Our ablation of different projection strength hyperparameter schedulers is shown below. For our systematic comparison against other methods for preserving pretrained representations, please see Appendix Sec. 9.

Comparison with different schedulers. We ablate the choice of scheduler and projection strength values in Table 6 on the LIBERO benchmark. Specifically, we compare against regular robust-finetuning (Constant scheduler), cosine scheduler and linear scheduler on projection strength values of 0.5, 2, and 3. We find that in general, project-strength modulation offers ID and OOD benefits compared to regular robust-finetuning. We also find that the linear scheduler offers most stable ID performance and greatest

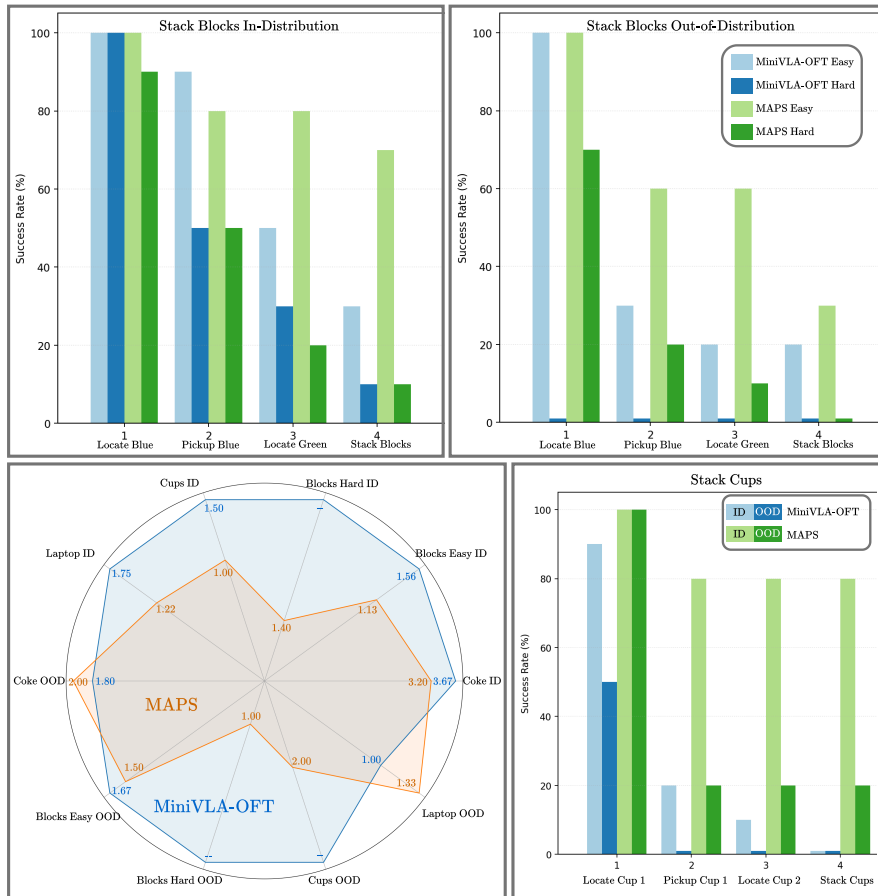


Figure 6. **Franka Detailed Results.** **Top Left:** Success rates for the Blocks ID Easy/Hard tasks. **Top Right:** Success rates for the Blocks OOD Easy/Hard tasks. **Bottom Left:** Average number of tries per success across all Franka tasks. **Bottom Right:** Success rates for the Cups ID/OOD tasks.

gains in OOD, with the best configuration being a linear scheduler with projection strength $v = 0.5$.

Table 6. **Scheduler Comparison:** Linear (MAPS, Ours) vs. Cosine (and Constant) across projection-strength values.

Scheduler / Value	ID		OOD				Avg. OOD
	LIBERO-90	-Spatial	-Object	-Goal	-Long		
Constant ($v=0.5$)	80	0	0	0	6	1.5	
Constant ($v=2$)	67	0	0	0	4	1	
Constant ($v=3$)	51	0	0	0	0	0	
Cosine ($v=0.5$)	81	0	2	0	6	2	
Cosine ($v=2$)	85	0	7	3	3	3.25	
Cosine ($v=3$)	87	0	9	1	2	3	
Linear ($v=0.5$)	88	0	7	6	6	4.75	
Linear ($v=2$)	84	2	6	0	4	3	
Linear ($v=3$)	88	1	2	0	6	2.25	

7. Conclusion

We present Module-Wise Proximity Scheduling (MAPS), a robust finetuning framework designed specifically for adapting pretrained VLM backbones to action data. By uncovering a clear hierarchy in how different model compo-

nents should be constrained, MAPS applies a linear scheduler that selectively regularizes each module. This yields conservative updates for visual layers – preserving essential geometric priors – while allowing more flexible adaptation in language components. Across SOTA backbones and standard benchmarks, MAPS delivers consistent improvements, enhancing both ID and OOD performance. Our findings highlight guided proximity to pretrained VLMs as a simple yet powerful principle for scalable VLA adaptation.

Acknowledgements. The authors gratefully acknowledge Jeremiah Coholich for his early contributions to the development of the Franka setup as well as support with the real robot experiments. This material is based upon work partially supported by the National Science Foundation under Grant No. 2239292. This research was also supported in part by Lambda, Inc. and through research cyberinfrastructure resources and services provided by the Partnership for an Advanced Computing Environment (PACE) at the Georgia Institute of Technology, Atlanta, Georgia, USA.

References

- [1] Moo Jin Kim, Karl Pertsch, Siddharth Karamcheti, Ted Xiao, Ashwin Balakrishna, Suraj Nair, Rafael Rafailov, Ethan Foster, Grace Lam, Pannag Sanketi, Quan Vuong, Thomas Kollar, Benjamin Burchfiel, Russ Tedrake, Dorsa Sadigh, Sergey Levine, Percy Liang, and Chelsea Finn. Openvla: An open-source vision-language-action model, 2024. URL <https://arxiv.org/abs/2406.09246>. 1, 2, 4
- [2] Anthony Brohan, Noah Brown, Justice Carbajal, Yevgen Chebotar, Joseph Dabis, Chelsea Finn, Keerthana Gopalakrishnan, Karol Hausman, Alex Herzog, Jasmine Hsu, Julian Ibarz, Brian Ichter, Alex Irpan, Tomas Jackson, Sally Jesmonth, Nikhil J Joshi, Ryan Julian, Dmitry Kalashnikov, Yuheng Kuang, Isabel Leal, Kuang-Huei Lee, Sergey Levine, Yao Lu, Utsav Malla, Deeksha Manjunath, Igor Mordatch, Ofir Nachum, Carolina Parada, Jodilyn Peralta, Emily Perez, Karl Pertsch, Jornell Quiambao, Kanishka Rao, Michael Ryoo, Grecia Salazar, Pannag Sanketi, Kevin Sayed, Jaspiar Singh, Sumedh Sontakke, Austin Stone, Clayton Tan, Huong Tran, Vincent Vanhoucke, Steve Vega, Quan Vuong, Fei Xia, Ted Xiao, Peng Xu, Sichun Xu, Tianhe Yu, and Brianna Zitkovich. Rt-1: Robotics transformer for real-world control at scale, 2023. URL <https://arxiv.org/abs/2212.06817>. 2, 7
- [3] Anthony Brohan, Noah Brown, Justice Carbajal, Yevgen Chebotar, Xi Chen, Krzysztof Choromanski, Tianli Ding, Danny Driess, Avinava Dubey, Chelsea Finn, Pete Florence, Chuyuan Fu, Montse Gonzalez Arenas, Keerthana Gopalakrishnan, Kehang Han, Karol Hausman, Alexander Herzog, Jasmine Hsu, Brian Ichter, Alex Irpan, Nikhil Joshi, Ryan Julian, Dmitry Kalashnikov, Yuheng Kuang, Isabel Leal, Lisa Lee, Tsang-Wei Edward Lee, Sergey Levine, Yao Lu, Henryk Michalewski, Igor Mordatch, Karl Pertsch, Kanishka Rao, Krista Reymann, Michael Ryoo, Grecia Salazar, Pannag Sanketi, Pierre Sermanet, Jaspiar Singh, Anikait Singh, Radu Soricut, Huong Tran, Vincent Vanhoucke, Quan Vuong, Ayzaan Wahid, Stefan Welker, Paul Wohlhart, Jialin Wu, Fei Xia, Ted Xiao, Peng Xu, Sichun Xu, Tianhe Yu, and Brianna Zitkovich. Rt-2: Vision-language-action models transfer web knowledge to robotic control, 2023. URL <https://arxiv.org/abs/2307.15818>. 2
- [4] Kevin Black, Noah Brown, Danny Driess, Adnan Esmail, Michael Equi, Chelsea Finn, Niccolo Fusai, Lachy Groom, Karol Hausman, Brian Ichter, Szymon Jakubczak, Tim Jones, Liyiming Ke, Sergey Levine, Adrian Li-Bell, Mohith Mothukuri, Suraj Nair, Karl Pertsch, Lucy Xiaoyang Shi, James Tanner, Quan Vuong, Anna Walling, Haohuan Wang, and Ury Zhilinsky. π_0 : A vision-language-action flow model for general robot control, 2024. URL <https://arxiv.org/abs/2410.24164>. 1, 2, 7
- [5] Lucas Beyer, Andreas Steiner, André Susano Pinto, Alexander Kolesnikov, Xiao Wang, Daniel Salz, Maxim Neumann, Ibrahim Alabdulmohsin, Michael Tschannen, Emanuele Bugliarelli, Thomas Unterthiner, Daniel Keysers, Skanda Koppula, Fangyu Liu, Adam Grycner, Alexey Gritsenko, Neil Houlsby, Manoj Kumar, Keran Rong, Julian Eisen-schlos, Rishabh Kabra, Matthias Bauer, Matko Bošnjak, Xi Chen, Matthias Minderer, Paul Voigtlaender, Ioana Bica, Ivana Balazevic, Joan Puigcerver, Pinelopi Papalampidi, Olivier Henaff, Xi Xiong, Radu Soricut, Jeremiah Harmsen, and Xiaohua Zhai. Paligemma: A versatile 3b vlm for transfer, 2024. URL <https://arxiv.org/abs/2407.07726>. 1, 2
- [6] Shuai Bai, Keqin Chen, Xuejing Liu, Jialin Wang, Wenbin Ge, Sibao Song, Kai Dang, Peng Wang, Shijie Wang, Jun Tang, Humen Zhong, Yuanzhi Zhu, Mingkun Yang, Zhao-hai Li, Jianqiang Wan, Pengfei Wang, Wei Ding, Zheren Fu, Yiheng Xu, Jiabo Ye, Xi Zhang, Tianbao Xie, Zesen Cheng, Hang Zhang, Zhibo Yang, Haiyang Xu, and Jun-yang Lin. Qwen2.5-vl technical report, 2025. URL <https://arxiv.org/abs/2502.13923>. 6
- [7] Hugo Touvron, Louis Martin, Kevin Stone, Peter Albert, Amjad Almahairi, Yasmine Babaei, Nikolay Bashlykov, Soumya Batra, Prajjwal Bhargava, Shruiti Bhosale, Dan Bikel, Lukas Blecher, Cristian Canton Ferrer, Moya Chen, Guillem Cucurull, David Esiobu, Jude Fernandes, Jeremy Fu, Wenyin Fu, Brian Fuller, Cynthia Gao, Vedanuj Goswami, Naman Goyal, Anthony Hartshorn, Saghar Hosseini, Rui Hou, Hakan Inan, Marcin Kardas, Viktor Kerkez, Madian Khabsa, Isabel Kloumann, Artem Korenev, Punit Singh Koura, Marie-Anne Lachaux, Thibaut Lavril, Jenya Lee, Diana Liskovich, Yinghai Lu, Yuning Mao, Xavier Martinet, Todor Mihaylov, Pushkar Mishra, Igor Molybog, Yixin Nie, Andrew Poulton, Jeremy Reizenstein, Rashi Rungta, Kalyan Saladi, Alan Schelten, Ruan Silva, Eric Michael Smith, Ranjan Subramanian, Xiaoqing Ellen Tan, Binh Tang, Ross Taylor, Adina Williams, Jian Xiang Kuan, Puxin Xu, Zheng Yan, Iliyan Zarov, Yuchen Zhang, Angela Fan, Melanie Kambadur, Sharan Narang, Aurelien Rodriguez, Robert Stojnic, Sergey Edunov, and Thomas Scialom. Llama 2: Open foundation and fine-tuned chat models, 2023. URL <https://arxiv.org/abs/2307.09288>. 1, 2, 3, 6
- [8] Sombit Dey, Jan-Nico Zaeck, Nikolay Nikolov, Luc Van Gool, and Danda Pani Paudel. Revla: Reverting visual domain limitation of robotic foundation models, 2024. URL <https://arxiv.org/abs/2409.15250>. 1, 2, 4, 3
- [9] Shresth Grover, Akshay Gopalkrishnan, Bo Ai, Henrik I. Christensen, Hao Su, and Xuanlin Li. Enhancing generalization in vision-language-action models by preserving pre-trained representations, 2025. URL <https://arxiv.org/abs/2509.11417>. 1, 2, 4, 3
- [10] Junjiao Tian, Xiaoliang Dai, Chih-Yao Ma, Zecheng He, Yen-Cheng Liu, and Zsolt Kira. Trainable projected gradient method for robust fine-tuning, 2023. URL <https://arxiv.org/abs/2303.10720>. 1, 2, 3
- [11] Maxime Oquab, Timothée Darcet, Théo Moutakanni, Huy Vo, Marc Szafraniec, Vasil Khalidov, Pierre Fernandez, Daniel Haziza, Francisco Massa, Alaaeldin El-Nouby, Mahmoud Assran, Nicolas Ballas, Wojciech Galuba, Russell Howes, Po-Yao Huang, Shang-Wen Li, Ishan Misra, Michael Rabbat, Vasu Sharma, Gabriel Synnaeve, Hu Xu, Hervé Jegou, Julien Mairal, Patrick Labatut, Armand Joulin, and Piotr Bojanowski. Dinov2: Learning robust visual features

- without supervision, 2024. URL <https://arxiv.org/abs/2304.07193>. 2, 3, 4
- [12] Xiaohua Zhai, Basil Mustafa, Alexander Kolesnikov, and Lucas Beyer. Sigmoid loss for language image pre-training, 2023. URL <https://arxiv.org/abs/2303.15343>. 2, 3
- [13] Junjiao Tian, Chengyue Huang, and Zsolt Kira. Rethinking weight decay for robust fine-tuning of foundation models, 2024. URL <https://arxiv.org/abs/2411.01713>. 2, 3
- [14] Xuhong Li, Yves Grandvalet, and Franck Davoine. Explicit inductive bias for transfer learning with convolutional networks, 2018. URL <https://arxiv.org/abs/1802.01483>. 3
- [15] Junjiao Tian, Yen-Cheng Liu, James Seale Smith, and Zsolt Kira. Fast trainable projection for robust fine-tuning, 2023. URL <https://arxiv.org/abs/2310.19182>. 2, 3
- [16] Henry Gouk, Eibe Frank, Bernhard Pfahringer, and Michael J. Cree. Regularisation of neural networks by enforcing lipschitz continuity, 2020. URL <https://arxiv.org/abs/1804.04368>. 2
- [17] Suneel Belkhale and Dorsa Sadigh. Minivla: A better vla with a smaller footprint, 2024. URL <https://github.com/Stanford-ILIAD/openvla-mini>. 2, 4, 6, 7, 8
- [18] Seungjae Lee, Yibin Wang, Haritheja Etukuru, H. Jin Kim, Nur Muhammad Mahi Shafiullah, and Lerrel Pinto. Behavior generation with latent actions, 2024. URL <https://arxiv.org/abs/2403.03181>. 2, 6
- [19] Moo Jin Kim, Chelsea Finn, and Percy Liang. Fine-tuning vision-language-action models: Optimizing speed and success, 2025. URL <https://arxiv.org/abs/2502.19645>. 2, 3, 6, 7
- [20] Xuanlin Li, Kyle Hsu, Jiayuan Gu, Karl Pertsch, Oier Mees, Homer Rich Walke, Chuyuan Fu, Ishikaa Lunawat, Isabel Sieh, Sean Kirmani, Sergey Levine, Jiajun Wu, Chelsea Finn, Hao Su, Quan Vuong, and Ted Xiao. Evaluating real-world robot manipulation policies in simulation, 2024. URL <https://arxiv.org/abs/2405.05941>. 2, 6
- [21] Oier Mees, Lukas Hermann, Erick Rosete-Beas, and Wolfram Burgard. Calvin: A benchmark for language-conditioned policy learning for long-horizon robot manipulation tasks, 2022. URL <https://arxiv.org/abs/2112.03227>. 2, 6
- [22] Bo Liu, Yifeng Zhu, Chongkai Gao, Yihao Feng, Qiang Liu, Yuke Zhu, and Peter Stone. Libero: Benchmarking knowledge transfer for lifelong robot learning, 2023. URL <https://arxiv.org/abs/2306.03310>. 2, 6
- [23] Alec Radford, Jong Wook Kim, Chris Hallacy, Aditya Ramesh, Gabriel Goh, Sandhini Agarwal, Girish Sastry, Amanda Askell, Pamela Mishkin, Jack Clark, Gretchen Krueger, and Ilya Sutskever. Learning transferable visual models from natural language supervision, 2021. URL <https://arxiv.org/abs/2103.00020>. 2
- [24] Danny Driess, Fei Xia, Mehdi S. M. Sajjadi, Corey Lynch, Aakanksha Chowdhery, Brian Ichter, Ayzaan Wahid, Jonathan Tompson, Quan Vuong, Tianhe Yu, Wenlong Huang, Yevgen Chebotar, Pierre Sermanet, Daniel Duckworth, Sergey Levine, Vincent Vanhoucke, Karol Hausman, Marc Toussaint, Klaus Greff, Andy Zeng, Igor Mordatch, and Pete Florence. Palm-e: An embodied multimodal language model, 2023. URL <https://arxiv.org/abs/2303.03378>. 2
- [25] Embodiment Collaboration, Abby O’Neill, Abdul Rehman, Abhinav Gupta, Abhiram Maddukuri, Abhishek Gupta, Abhishek Padalkar, Abraham Lee, Acorn Pooley, Agrim Gupta, Ajay Mandlekar, Ajinkya Jain, Albert Tung, Alex Bewley, Alex Herzog, Alex Irpan, Alexander Khazatsky, Anant Rai, Anchit Gupta, Andrew Wang, Andrey Kolobov, Anikait Singh, Animesh Garg, Aniruddha Kembhavi, Annie Xie, Anthony Brohan, Antonin Raffin, Archit Sharma, Arefeh Yavary, Arhan Jain, Ashwin Balakrishna, Ayzaan Wahid, Ben Burgess-Limerick, Beomjoon Kim, Bernhard Schölkopf, Blake Wulfe, Brian Ichter, Cewu Lu, Charles Xu, Charlotte Le, Chelsea Finn, Chen Wang, Chenfeng Xu, Cheng Chi, Chenguang Huang, Christine Chan, Christopher Agia, Chuer Pan, Chuyuan Fu, Coline Devin, Danfei Xu, Daniel Morton, Danny Driess, Daphne Chen, Deepak Pathak, Dhruv Shah, Dieter Büchler, Dinesh Jayaraman, Dmitry Kalashnikov, Dorsa Sadigh, Edward Johns, Ethan Foster, Fangchen Liu, Federico Ceola, Fei Xia, Feiyu Zhao, Felipe Vieira Frujeri, Freek Stulp, Gaoyue Zhou, Gaurav S. Sukhatme, Gautam Salhotra, Ge Yan, Gilbert Feng, Giulio Schiavi, Glen Berseth, Gregory Kahn, Guangwen Yang, Guanzhi Wang, Hao Su, Hao-Shu Fang, Haochen Shi, Henghui Bao, Heni Ben Amor, Henrik I Christensen, Hiroki Furuta, Homanga Bharadhwaj, Homer Walke, Hongjie Fang, Huy Ha, Igor Mordatch, Ilija Radosavovic, Isabel Leal, Jacky Liang, Jad Abou-Chakra, Jaehyung Kim, Jaimyn Drake, Jan Peters, Jan Schneider, Jasmine Hsu, Jay Vakil, Jeannette Bohg, Jeffrey Bingham, Jeffrey Wu, Jensen Gao, Jiaheng Hu, Jiajun Wu, Jialin Wu, Jiankai Sun, Jianlan Luo, Jiayuan Gu, Jie Tan, Jihoon Oh, Jimmy Wu, Jingpei Lu, Jingyun Yang, Jitendra Malik, João Silvério, Joey Heyna, Jonathan Booher, Jonathan Tompson, Jonathan Yang, Jordi Salvador, Joseph J. Lim, Junhyek Han, Kaiyuan Wang, Kanishka Rao, Karl Pertsch, Karol Hausman, Keegan Go, Keerthana Gopalakrishnan, Ken Goldberg, Kendra Byrne, Kenneth Oslund, Kento Kawaharazuka, Kevin Black, Kevin Lin, Kevin Zhang, Kiana Ehsani, Kiran Lekkala, Kirsty Ellis, Krishan Rana, Krishnan Srinivasan, Kuan Fang, Kunal Pratap Singh, Kuo-Hao Zeng, Kyle Hatch, Kyle Hsu, Laurent Itti, Lawrence Yunliang Chen, Lerrel Pinto, Li Fei-Fei, Liam Tan, Linxi ”Jim” Fan, Lionel Ott, Lisa Lee, Luca Weihs, Magnum Chen, Marion Lepert, Marius Memmel, Masayoshi Tomizuka, Masha Itkina, Mateo Guaman Castro, Max Spero, Maximilian Du, Michael Ahn, Michael C. Yip, Mingtong Zhang, Mingyu Ding, Minh Heo, Mohan Kumar Srirama, Mohit Sharma, Moo Jin Kim, Muhammad Zubair Irshad, Naoaki Kanazawa, Nicklas Hansen, Nicolas Heess, Nikhil J Joshi, Niko Suenderhauf, Ning Liu, Norman Di Palo, Nur Muhammad Mahi Shafiullah, Oier Mees, Oliver Kroemer, Osbert Bastani, Pannag R Sanketi, Patrick ”Tree” Miller, Patrick Yin, Paul Wohlhart, Peng Xu, Peter David Fagan, Peter Mitrano, Pierre Sermanet, Pieter Abbeel, Priya Sundaresan, Qiuyu Chen, Quan Vuong, Rafael Rafailov, Ran Tian, Ria Doshi, Roberto Martín-Martín, Ro-

- han Baijal, Rosario Scalise, Rose Hendrix, Roy Lin, Run-
 jia Qian, Ruohan Zhang, Russell Mendonca, Rutav Shah,
 Ryan Hoque, Ryan Julian, Samuel Bustamante, Sean Kir-
 mani, Sergey Levine, Shan Lin, Sherry Moore, Shikhar Bahl,
 Shivin Dass, Shubham Sonawani, Shubham Tulsiani, Shu-
 ran Song, Sichun Xu, Siddhant Haldar, Siddharth Karam-
 cheti, Simeon Adebola, Simon Guist, Soroush Nasiriany,
 Stefan Schaal, Stefan Welker, Stephen Tian, Subramanian
 Ramamoorthy, Sudeep Dasari, Suneel Belkhale, Sungjae
 Park, Suraj Nair, Suvir Mirchandani, Takayuki Osa, Tan-
 may Gupta, Tatsuya Harada, Tatsuya Matsushima, Ted Xiao,
 Thomas Kollar, Tianhe Yu, Tianli Ding, Todor Davchev,
 Tony Z. Zhao, Travis Armstrong, Trevor Darrell, Trinity
 Chung, Vidhi Jain, Vikash Kumar, Vincent Vanhoucke, Vi-
 ctor Guizilini, Wei Zhan, Wenxuan Zhou, Wolfram Burgard,
 Xi Chen, Xiangyu Chen, Xiaolong Wang, Xinghao Zhu,
 Xinyang Geng, Xiyuan Liu, Xu Liangwei, Xuanlin Li, Yan-
 song Pang, Yao Lu, Yecheng Jason Ma, Yejin Kim, Yev-
 gen Chebotar, Yifan Zhou, Yifeng Zhu, Yilin Wu, Ying Xu,
 Yixuan Wang, Yonatan Bisk, Yongqiang Dou, Yoonyoung
 Cho, Youngwoon Lee, Yuchen Cui, Yue Cao, Yueh-Hua
 Wu, Yujin Tang, Yuke Zhu, Yunchu Zhang, Yunfan Jiang,
 Yunshuang Li, Yunzhu Li, Yusuke Iwasawa, Yutaka Mat-
 suo, Zehan Ma, Zhuo Xu, Zichen Jeff Cui, Zichen Zhang,
 Zipeng Fu, and Zipeng Lin. Open x-embodiment: Robotic
 learning datasets and rt-x models, 2025. URL <https://arxiv.org/abs/2310.08864>. 2
- [26] Physical Intelligence, Kevin Black, Noah Brown, James
 Darpinian, Karan Dhabalia, Danny Driess, Adnan Esmail,
 Michael Equi, Chelsea Finn, Niccolo Fusai, Manuel Y. Gal-
 liker, Dibya Ghosh, Lachy Groom, Karol Hausman, Brian
 Ichter, Szymon Jakubczak, Tim Jones, Liyiming Ke, Devin
 LeBlanc, Sergey Levine, Adrian Li-Bell, Mohith Mothukuri,
 Suraj Nair, Karl Pertsch, Allen Z. Ren, Lucy Xiaoyang Shi,
 Laura Smith, Jost Tobias Springenberg, Kyle Stachowicz,
 James Tanner, Quan Vuong, Homer Walke, Anna Walling,
 Haohuan Wang, Lili Yu, and Ury Zhilinsky. $\pi_{0.5}$: a
 vision-language-action model with open-world generaliza-
 tion, 2025. URL <https://arxiv.org/abs/2504.16054>.
- [27] Danny Driess, Jost Tobias Springenberg, Brian Ichter, Lili
 Yu, Adrian Li-Bell, Karl Pertsch, Allen Z. Ren, Homer
 Walke, Quan Vuong, Lucy Xiaoyang Shi, and Sergey Levine.
 Knowledge insulating vision-language-action models: Train
 fast, run fast, generalize better, 2025. URL <https://arxiv.org/abs/2505.23705>. 2
- [28] Andrew Szot, Bogdan Mazouze, Harsh Agrawal, R Devon
 Hjelm, Zsolt Kira, and Alexander Toshev. Grounding multi-
 modal large language models in actions. *Advances in Neural
 Information Processing Systems*, 37:20198–20224, 2024. 2
- [29] Karl Pertsch, Kyle Stachowicz, Brian Ichter, Danny Driess,
 Suraj Nair, Quan Vuong, Oier Mees, Chelsea Finn, and
 Sergey Levine. Fast: Efficient action tokenization for vision-
 language-action models, 2025. URL <https://arxiv.org/abs/2501.09747>. 3
- [30] Suneel Belkhale, Tianli Ding, Ted Xiao, Pierre Sermanet,
 Quon Vuong, Jonathan Tompson, Yevgen Chebotar, De-
 bidatta Dwibedi, and Dorsa Sadigh. Rt-h: Action hierarchies
 using language, 2024. URL <https://arxiv.org/abs/2403.01823>.
- [31] Tony Z. Zhao, Vikash Kumar, Sergey Levine, and Chelsea
 Finn. Learning fine-grained bimanual manipulation with
 low-cost hardware, 2023. URL <https://arxiv.org/abs/2304.13705>.
- [32] Moritz Reuss, Hongyi Zhou, Marcel Rühle, Ömer Erdiç
 Yağmurlu, Fabian Otto, and Rudolf Lioutikov. FLOWER:
 Democratizing generalist robot policies with efficient vision-
 language-flow models. In *9th Annual Conference on Robot
 Learning*, 2025. URL <https://openreview.net/forum?id=JeppaebLRD>. 2
- [33] Mustafa Shukor, Dana Aubakirova, Francesco Capuano,
 Pepijn Kooijmans, Steven Palma, Adil Zouitine, Michel Ar-
 actingi, Caroline Pascal, Martino Russi, Andres Marafioti,
 Simon Alibert, Matthieu Cord, Thomas Wolf, and Remi Ca-
 dene. Smolvla: A vision-language-action model for afford-
 able and efficient robotics, 2025. URL <https://arxiv.org/abs/2506.01844>. 2
- [34] Junjie Wen, Yichen Zhu, Jinming Li, Minjie Zhu, Kun Wu,
 Zhiyuan Xu, Ning Liu, Ran Cheng, Chaomin Shen, Yaxin
 Peng, Feifei Feng, and Jian Tang. Tinyvla: Towards fast,
 data-efficient vision-language-action models for robotic ma-
 nipulation, 2025. URL <https://arxiv.org/abs/2409.12514>. 2
- [35] Zhongyi Zhou, Yichen Zhu, Minjie Zhu, Junjie Wen,
 Ning Liu, Zhiyuan Xu, Weibin Meng, Ran Cheng, Yaxin
 Peng, Chaomin Shen, and Feifei Feng. Chatvla: Unified
 multimodal understanding and robot control with vision-
 language-action model, 2025. URL <https://arxiv.org/abs/2502.14420>. 2
- [36] Zhongyi Zhou, Yichen Zhu, Junjie Wen, Chaomin Shen,
 and Yi Xu. Chatvla-2: Vision-language-action model with
 open-world embodied reasoning from pretrained knowl-
 edge, 2025. URL <https://arxiv.org/abs/2505.21906>.
- [37] Lucy Xiaoyang Shi, Brian Ichter, Michael Equi, Liyim-
 ing Ke, Karl Pertsch, Quan Vuong, James Tanner, Anna
 Walling, Haohuan Wang, Niccolo Fusai, Adrian Li-Bell,
 Danny Driess, Lachy Groom, Sergey Levine, and Chelsea
 Finn. Hi robot: Open-ended instruction following with
 hierarchical vision-language-action models, 2025. URL
<https://arxiv.org/abs/2502.19417>.
- [38] Jason Lee, Jiafei Duan, Haoquan Fang, Yuquan Deng, Shuo
 Liu, Boyang Li, Bohan Fang, Jieyu Zhang, Yi Ru Wang,
 Sangho Lee, Winson Han, Wilbert Pumacay, Angelica Wu,
 Rose Hendrix, Karen Farley, Eli VanderBilt, Ali Farhadi, Di-
 eter Fox, and Ranjay Krishna. Molmoact: Action reason-
 ing models that can reason in space, 2025. URL <https://arxiv.org/abs/2508.07917>.
- [39] Delin Qu, Haoming Song, Qizhi Chen, Yuanqi Yao, Xinyi
 Ye, Yan Ding, Zhigang Wang, JiaYuan Gu, Bin Zhao, Dong
 Wang, and Xuelong Li. Spatialvla: Exploring spatial rep-
 resentations for visual-language-action model, 2025. URL
<https://arxiv.org/abs/2501.15830>.
- [40] Yang Tian, Sizhe Yang, Jia Zeng, Ping Wang, Dahua Lin,
 Hao Dong, and Jiangmiao Pang. Predictive inverse dynamics

- models are scalable learners for robotic manipulation, 2024. URL <https://arxiv.org/abs/2412.15109>.
- [41] Andrew Szot, Bogdan Mazoure, Omar Attia, Aleksei Timofeev, Harsh Agrawal, Devon Hjelm, Zhe Gan, Zsolt Kira, and Alexander Toshev. From multimodal llms to generalist embodied agents: Methods and lessons. In *Proceedings of the Computer Vision and Pattern Recognition Conference*, pages 10644–10655, 2025. 2
- [42] Qingqing Zhao, Yao Lu, Moo Jin Kim, Zipeng Fu, Zhuoyang Zhang, Yecheng Wu, Zhaoshuo Li, Qianli Ma, Song Han, Chelsea Finn, Ankur Handa, Ming-Yu Liu, Donglai Xiang, Gordon Wetzstein, and Tsung-Yi Lin. Cot-vla: Visual chain-of-thought reasoning for vision-language-action models, 2025. URL <https://arxiv.org/abs/2503.22020>. 2
- [43] Michał Zawalski, William Chen, Karl Pertsch, Oier Mees, Chelsea Finn, and Sergey Levine. Robotic control via embodied chain-of-thought reasoning, 2025. URL <https://arxiv.org/abs/2407.08693>.
- [44] Junjie Wen, Minjie Zhu, Yichen Zhu, Zhibin Tang, Jinming Li, Zhongyi Zhou, Chengmeng Li, Xiaoyu Liu, Yaxin Peng, Chaomin Shen, and Feifei Feng. Diffusion-vla: Generalizable and interpretable robot foundation model via self-generated reasoning, 2025. URL <https://arxiv.org/abs/2412.03293>. 2
- [45] Ji Zhang, Shihan Wu, Xu Luo, Hao Wu, Lianli Gao, Heng Tao Shen, and Jingkuan Song. Inspire: Vision-language-action models with intrinsic spatial reasoning, 2025. URL <https://arxiv.org/abs/2505.13888>. 2
- [46] Asher J. Hancock, Xindi Wu, Lihan Zha, Olga Russakovsky, and Anirudha Majumdar. Actions as language: Fine-tuning vlms into vlas without catastrophic forgetting, 2025. URL <https://arxiv.org/abs/2509.22195>. 2
- [47] Huang Huang, Fangchen Liu, Letian Fu, Tingfan Wu, Mustafa Mukadam, Jitendra Malik, Ken Goldberg, and Pieter Abbeel. Otter: A vision-language-action model with text-aware visual feature extraction, 2025. URL <https://arxiv.org/abs/2503.03734>. 2
- [48] Nikita Kachaev, Mikhail Kolosov, Daniil Zelezetsky, Alexey K. Kovalev, and Aleksandr I. Panov. Don’t blind your vla: Aligning visual representations for ood generalization, 2025. URL <https://arxiv.org/abs/2510.25616>. 2, 4
- [49] Jianing Guo, Zhenhong Wu, Chang Tu, Yiyao Ma, Xiangqi Kong, Zhiqian Liu, Jiaming Ji, Shuning Zhang, Yuanpei Chen, Kai Chen, Qi Dou, Yaodong Yang, Xianglong Liu, Huijie Zhao, Weifeng Lv, and Simin Li. On robustness of vision-language-action model against multi-modal perturbations, 2025. URL <https://arxiv.org/abs/2510.00037>. 2
- [50] Chengyue Huang, Junjiao Tian, Brisa Maneechotesuwan, Shivang Chopra, and Zsolt Kira. Directional gradient projection for robust fine-tuning of foundation models, 2025. URL <https://arxiv.org/abs/2502.15895>. 3
- [51] Chengyue Huang, Brisa Maneechotesuwan, Shivang Chopra, and Zsolt Kira. Frames-vqa: Benchmarking fine-tuning robustness across multi-modal shifts in visual question answering, 2025. URL <https://arxiv.org/abs/2505.21755>. 3
- [52] Siddharth Karamcheti, Suraj Nair, Ashwin Balakrishna, Percy Liang, Thomas Kollar, and Dorsa Sadigh. Prismatic vlms: Investigating the design space of visually-conditioned language models, 2024. URL <https://arxiv.org/abs/2402.07865>. 4
- [53] Yihao Wang, Pengxiang Ding, Lingxiao Li, Can Cui, Zirui Ge, Xinyang Tong, Wenxuan Song, Han Zhao, Wei Zhao, Pengxu Hou, Siteng Huang, Yifan Tang, Wenhui Wang, Ru Zhang, Jianyi Liu, and Donglin Wang. Vla-adapter: An effective paradigm for tiny-scale vision-language-action model, 2025. URL <https://arxiv.org/abs/2509.09372>. 4, 6, 8, 2
- [54] Octo Model Team, Dibya Ghosh, Homer Walke, Karl Pertsch, Kevin Black, Oier Mees, Sudeep Dasari, Joey Hejna, Tobias Kreiman, Charles Xu, Jianlan Luo, You Liang Tan, Lawrence Yunliang Chen, Pannag Sanketi, Quan Vuong, Ted Xiao, Dorsa Sadigh, Chelsea Finn, and Sergey Levine. Octo: An open-source generalist robot policy, 2024. URL <https://arxiv.org/abs/2405.12213>. 7
- [55] Cunxin Fan, Xiaosong Jia, Yihang Sun, Yixiao Wang, Jianglan Wei, Ziyang Gong, Xiangyu Zhao, Masayoshi Tomizuka, Xue Yang, Junchi Yan, and Mingyu Ding. Interleave-vla: Enhancing robot manipulation with interleaved image-text instructions, 2025. URL <https://arxiv.org/abs/2505.02152>. 6, 7
- [56] Jeremiah Coholich, Justin Wit, and Zsolt Kira. Sim2real image translation enables viewpoint-robust policies from fixed-camera datasets. In *Proceedings of the 6th Annual Embodied AI Workshop (EAI) at the IEEE/CVF Conference on Computer Vision and Pattern Recognition (CVPR)*, Nashville, Tennessee, USA, June 2025. URL https://www.jeremiahcoholich.com/publication/iros_2025/CVPR_EAI_Workshop_2025.pdf. 8

MAPS: Preserving Vision-Language Representations via Module-Wise Proximity Scheduling for Better Vision-Language-Action Generalization

Supplementary Material

8. Performance on Real-World Franka Emika Panda Robot

8.1. Experiment Setting

Hardware Setup. We conduct real-world tabletop manipulation experiments using a single Franka Emika Panda robotic arm and two RealSense D435 cameras, one mounted in a third perspective and one mounted as a wrist camera (Fig. 7). The cameras capture images in 1920×1080 resolution, which is resized and center-cropped to construct 224×224 resolution inputs for training and inference.

Experiment Setup. We design 4 task settings:

1. Coke: grab the coke can and lift it up,
2. Blocks: stack the blue block on the green block,
3. Cups: stack the orange cup onto the green cup,
4. Laptop: close the laptop lid fully.

We evaluate each task setting using ten rollouts across two object–location configurations, with five rollouts per configuration. For the multi-object Blocks and Cups tasks, the second configuration is created by swapping the positions of the objects. For the Coke task, we use “near” and “far” layouts, placing the can either within the gripper’s immediate reach or farther away. For the Laptop task, the two configurations place the laptop at an acute 60° angle, oriented either toward or away from the camera. To enable a more fine-grained task analysis, we further introduce a Hard setting for the Blocks task, where objects are positioned farther from the robot arm (Fig. 8) while still relying on configurations that simply swap object positions. We also define a new out-of-distribution (OOD) variant for this Hard setting by replacing the blue block with a red one. This results in a substantially more challenging OOD condition than the original Easy OOD, as both the visual appearance and semantic attributes differ from the pretrained setup.

8.2. Qualitative Results

We show the qualitative results of ID and OOD tasks in Figs. 9 and 10, with raw video recordings of these rollouts included on our project site. Across both settings, MAPS and the baseline exhibit clear and consistent behavioral differences. The baseline policies frequently stall, hesitate, or follow incorrect trajectories, resulting in missed grasps, poor approach angles, unstable placements, or premature object drops. These failures are visible in Cup ID, Block ID, and Coke ID (Fig. 9), where the baseline often grasps imprecisely, retries multiple times (Block ID), tips objects over (Coke ID), or performs poor localization that

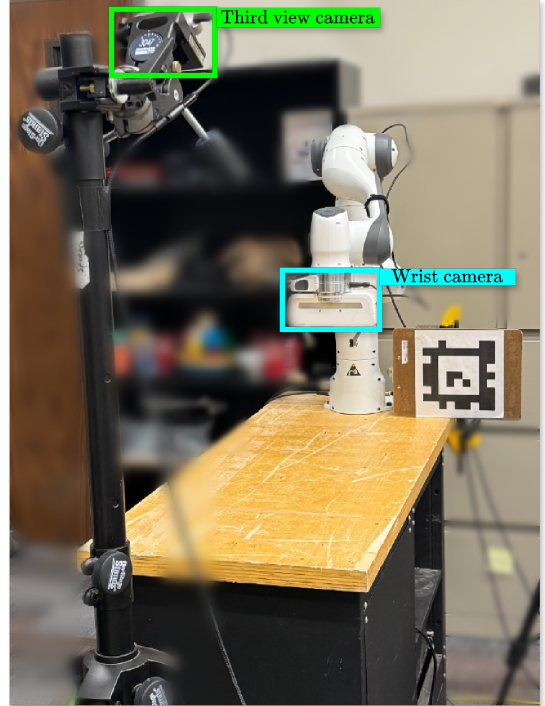


Figure 7. Franka Emika Panda Arm Experiment Setup.

causes early releases (Cup ID). In contrast, MAPS executes smoother, more deliberate, and more stable motion plans. It firmly grasps objects, recalibrates effectively to locate secondary targets, and demonstrates careful multi-step execution – such as reopening and reclosing the gripper when the orange cup initially fails to stack into the green cup – without letting objects fall.

These qualitative differences become even more pronounced under distribution shifts (Fig. 10). MAPS consistently adapts to altered object appearances and dynamics, whereas the baseline tends to rigidly reuse its ID trajectories and fails to compensate for changes. In Laptop OOD, replacing the Alienware laptop with a MacBook Pro introduces greater joint friction; the baseline follows its original trajectory and leaves the MacBook partially open (10–30%), while MAPS adopts a more conservative path and applies sufficient, consistent force to close it fully. A similar pattern appears in Block OOD, where the first block’s elevation is altered. MAPS successfully adjusts its grasp strategy, while the baseline struggles and persists with its ID motion. Taken together, these visual rollouts show that MAPS not only corrects common baseline failure

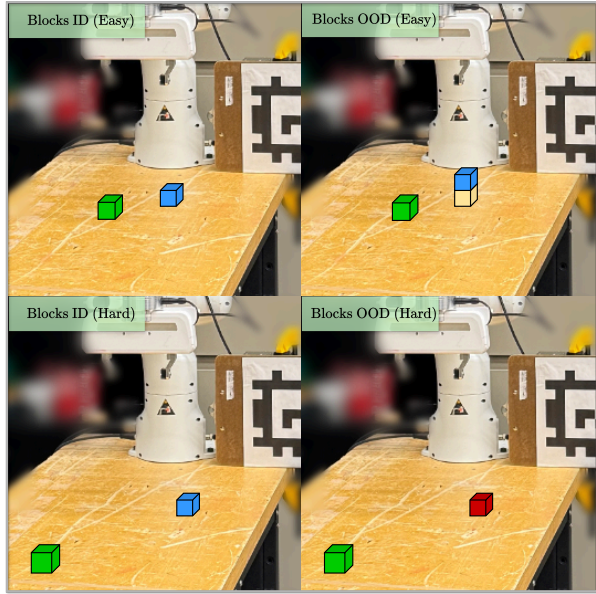


Figure 8. **Task 2 (Block) settings.** To further differentiate between MAPS and the baseline MiniVLA-OFT, we construct a more challenging “Hard” variant of T2: Block by introducing more geometric and vision variations. Blocks ID Hard (bottom left) increases the separation between the two blocks to probe long range planning and task execution, whereas Blocks OOD Hard (bottom right) additionally introduces an unseen new color block to the task.

modes but also exhibits markedly stronger robustness, carefulness, and adaptability in both familiar and shifted environments.

8.3. Results Discussion

We discuss some questions regarding our qualitative and quantitative results.

(1) Why are the performance gains on our real world ID evaluations so much more pronounced compared to our simulation ID results in the main paper? One of our central hypotheses for the large ID performance gap on Franka is the limited size of our pretraining dataset – only 600 demonstrations – which likely leads to substantial overfitting in the baseline model. Both our qualitative observations and quantitative OOD results already indicate that the baseline MiniVLA-OFT is highly sensitive to spurious correlations. We believe the baseline has overfit so strongly to the demonstration distribution that minor natural variations which should remain well within the ID regime become challenging for it to handle. In contrast, the regularization introduced by MAPS mitigates this overfitting, enabling the model to generalize more robustly.

(2) Why, in general, are these success rates the way that they are? Across our tasks, a consistent trend emerges: grasping is challenging, and grasping round objects is especially difficult. In contrast, the Laptop task is comparatively

trivial because it only requires the robot arm to push the object along a trajectory rather than perform a true grasp. The Block task is easier than Cup because the block’s square geometry provides stable grasping affordances. This explains why the baseline and MAPS perform similarly on Block grasping, whereas MAPS is substantially better on Cup grasping. As shown in Fig. 6, the baseline’s primary failure point on Blocks (ID) is in locating the second object, while on Cups (ID) the main dropoff occurs at the very first grasp. The Coke task also involves grasping a cylindrical object, but it is more straightforward than Cup because only a single grasp is required. Taken together, these observations suggest the following expected difficulty ordering: Cup > Block > Coke > Laptop. This is also consistent with our observed results.

(3) Why does MAPS perform worse on Laptop ID compared to baseline MiniVLA-OFT? On the Laptop ID/OOD tasks, we observed a recurring failure mode shared by both MAPS and the baseline, stemming partly from the task’s design. In configurations where the laptop screen faces the robot, once the arm pushes the lid down past a certain angle, the third-view camera can no longer reliably determine whether the laptop is fully closed. Because the learned policies typically lift the arm after pushing to avoid contacting the table, small partial closings also become indistinguishable from the wrist-view camera. The single MAPS ID failure arose from this ambiguity, and we observed similar issues in the OOD setting for both methods. Although one could debate how to interpret “success” for such borderline cases, we chose to evaluate results strictly and consistently. Overall, the Laptop task appears too saturated and simple to reveal meaningful differences in the ID setting – making a 10% change negligible – whereas the 30% gap in the OOD setting is far more consequential.

9. Comparison with Baselines

Table 7. **Dual Encoders vs. MAPS on LIBERO using MiniVLA-VQ.**

Method	LIBERO-90 (ID)	Avg. OOD	Params
MiniVLA-VQ (baseline) [53]	79	0.0	1.5B
+Dual-Encoder [9]	75	2.75	1.5B
+Dual-Encoder (new DINOv2+SigLIP)	79	3.75	2.5B
+MAPS (Ours)	82	4.75	1.5B

Comparison with Dual Encoders. The comparison against different dual-encoder variants is presented in Tab. 7. Notably, MAPS achieves the strongest performance among all compared methods while remaining the most compute-efficient. Dual-encoder approaches require instantiating a second trainable copy of the frozen vision encoder, which effectively doubles the parameter count of the vision stack. We implement this as the **Dual-Encoder (new DI-**

NOv2+SigLIP) variant. A more efficient variant is proposed by [9], in which one of the vision encoders is frozen while the other is kept trainable. We implement this as the **Dual-Encoder** variant. As shown in the table, neither dual-encoder variant matches the ID or OOD performance of MAPS. **Dual-Encoder** performs worst, and **Dual-Encoder (new DINOv2+SigLIP)** is slightly better but incurs substantially higher architectural cost. MAPS offers the best performance without additional cost.

Comparison with Weight Interpolation. Weight interpolation methods such as [8] also introduces additional overhead: it depends on having a finetuned set of VLA weights available for interpolation, which means one training run to obtain those weights and another to perform the interpolation process.

Comparison with Bi-Level Optimization. Bi-level optimization approaches that hyper-optimize the constraints between the fine-tuned and pre-trained weights, such as [15], incur roughly twice the training time. Under this setting, the resulting policy attains 79% ID success and 4% OOD success using VLA-Adapter, and 0% ID and OOD success using MiniVLA-VQ, both of which fall short of MAPS while requiring significantly higher computational cost.

10. Configurations for each Benchmark/Model

In Tab. 8, we summarize the training configurations used across different models and benchmarks. Specifically, we report the optimal learning rate, total training steps, global batch size, usage of the wrist camera and proprioceptive state, whether image augmentation is applied, whether LoRA is used (and, if so, the chosen rank), the GPU setup, total training time, and the value of λ_{\max} used in MAPS.

11. Algorithm

The full algorithm of MAPS is shown in Algorithm 1. The algorithm extends standard Adam optimization with a progressive Module-Wise Proximity Scheduling regularization strategy applied across an ordered stack of model layers. Beginning with the lowest-level representation (DINOv2) and proceeding sequentially toward the highest-level language layers, the method assigns each layer a monotonically decreasing proximal weight λ_k , with the strongest regularization applied to early layers and no regularization applied to the final layer. For each layer, the algorithm performs standard Adam updates by computing stochastic gradients, maintaining exponential moving averages of first- and second-order moments, and applying bias correction before taking an adaptive step in parameter space. After each tentative Adam update $\hat{\theta}_t$, the method evaluates a MAPS consistency signal c_t , defined as the negative inner product between the current negative gradient $-g_t^T$ and the displacement from the initialization $\theta_{t-1} - \theta_0$. A negative

Algorithm 1: Adam with MAPS.

Given: ordered layer set
 $\mathcal{L} = (\text{DINOv2}, \text{SigLIP}, \text{Bridge}, \text{Language})$

Hyperparameters: $\alpha, \beta_1, \beta_2, \epsilon, \lambda_{\max}$

Pre-computation: For $k = 1, \dots, |\mathcal{L}|$ define

$$\lambda_k := \lambda_{\max} \left(1 - \frac{k-1}{|\mathcal{L}|-1} \right),$$

so that $\lambda_1 = \lambda_{\max}$ (DINOv2) and $\lambda_{|\mathcal{L}|} = 0$ (Language).

Initialization: $m_0 \leftarrow 0, v_0 \leftarrow 0, t \leftarrow 0, c_0 \leftarrow 0$

For $k = 1, \dots, |\mathcal{L}|$ (**from DINOv2 to Language**)

do

while θ_t not converged **do**

$t \leftarrow t + 1$

$g_t \leftarrow \nabla_{\theta} \tilde{\mathcal{L}}(\theta_{t-1})$

$m_t \leftarrow \beta_1 m_{t-1} + (1 - \beta_1) g_t$

$v_t \leftarrow \beta_2 v_{t-1} + (1 - \beta_2) g_t^2$

Bias correction:

$$\hat{m}_t \leftarrow \frac{m_t}{1 - \beta_1^t}, \quad \hat{v}_t \leftarrow \frac{v_t}{1 - \beta_2^t}$$

Adam update:

$$\tilde{\theta}_t \leftarrow \theta_{t-1} - \frac{\alpha \hat{m}_t}{\sqrt{\hat{v}_t} + \epsilon}$$

$c_t \leftarrow -g_t^T (\theta_{t-1} - \theta_0)$

If $c_t < 0$ **then**

$$\theta_t \leftarrow \tilde{\theta}_t - \lambda_k r_t (\tilde{\theta}_t - \theta_0)$$

else

$$\theta_t \leftarrow \tilde{\theta}_t$$

end if

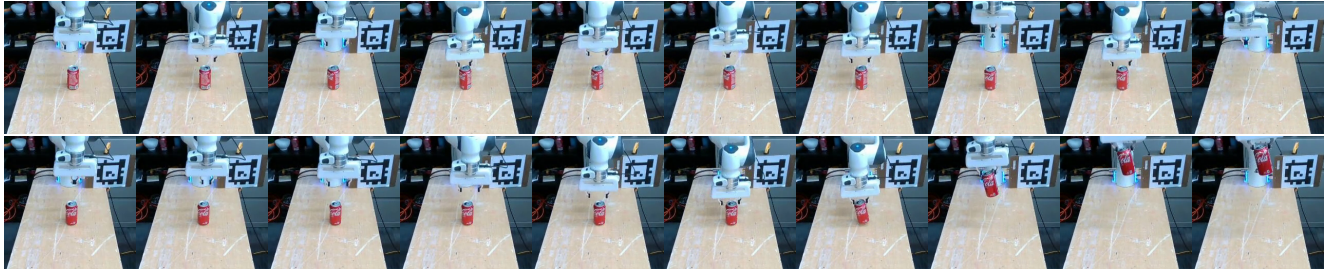
end while

end for

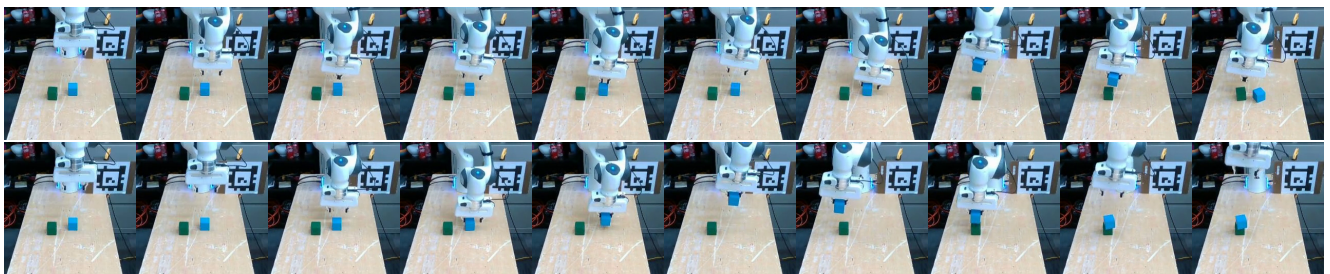
value indicates movement that contradicts the expected descent direction relative to the original initialization and triggers a correction: the updated parameters are pulled back toward the initialization by an amount proportional to both the layer-specific proximal weight λ_k and the deviation ratio r_t . If the consistency signal is non-negative, the Adam update is accepted unchanged. By iterating this procedure until convergence at each layer before progressing to the next, the algorithm preserves the stability of foundational layers and components (DINOv2 and SigLIP), encourages smooth and initialization-aligned updates in intermediate modules, and allows full flexibility in the final language components.

Table 8. Configurations for Each Model and Benchmark.

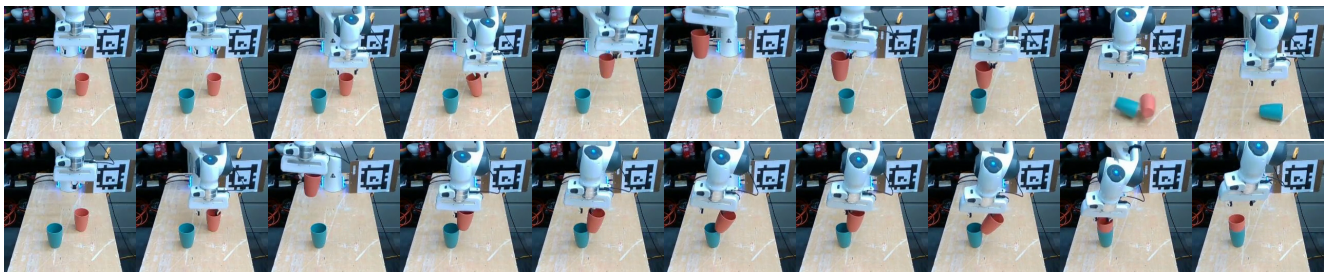
Benchmark	Model	lr	steps	batch size	use wrist	use proprio	use img aug	lora	GPUs	Training Time	λ_{\max}
LIBERO	MiniVLA-VQ	1e-5	50000	16*8	no	no	False	False	8*A40	24h	0.5
	MiniVLA-OFT	5e-5	50000	8*8	yes	yes	True	False	8*A40	19h	3.2
	VLA-Adapter	1e-4	50000	8*8	yes	yes	True	False	8*A40	22h	0.5
	OpenVLA-OFT	5e-5	50000	4*16	yes	yes	True	r=32	16*A40	28h	1.0
CALVIN	MiniVLA-OFT	5e-5	40000	8*8	yes	yes	True	False	8*A40	19h	2.5
	OpenVLA-OFT	1e-4	35000	4*16	yes	yes	True	r=32	16*A40	28h	1.5
SimplerEnv	MiniVLA-VQ	1e-5	50000	32*4	no	no	False	False	4*H200	10h	0.5
	MiniVLA-OFT	5e-5	100000	8*8	no	no	True	False	8*A40	15h	3.0
	OpenVLA-OFT	2e-4	100000	16*4	no	no	True	r=32	4*H200	21h	0.8
Franka	MiniVLA-OFT	5e-5	100000	8*8	yes	no	True	False	8*A40	14h	1.5



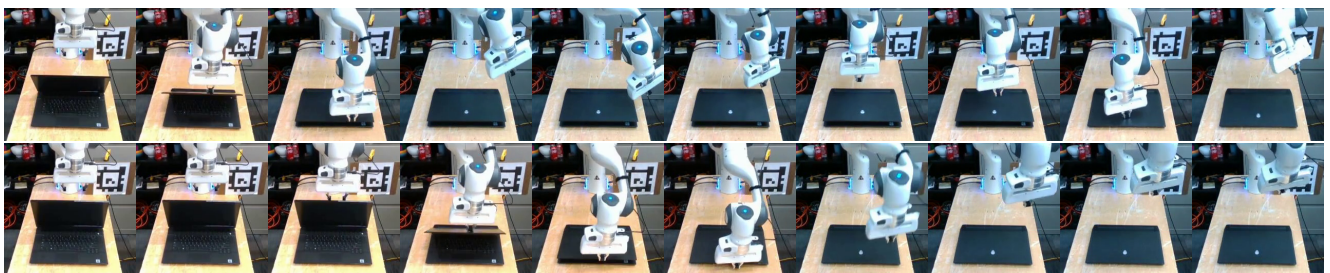
(1) Grab the Coke Can and Lift It Up



(2) Stack the Blue Block on the Green Block

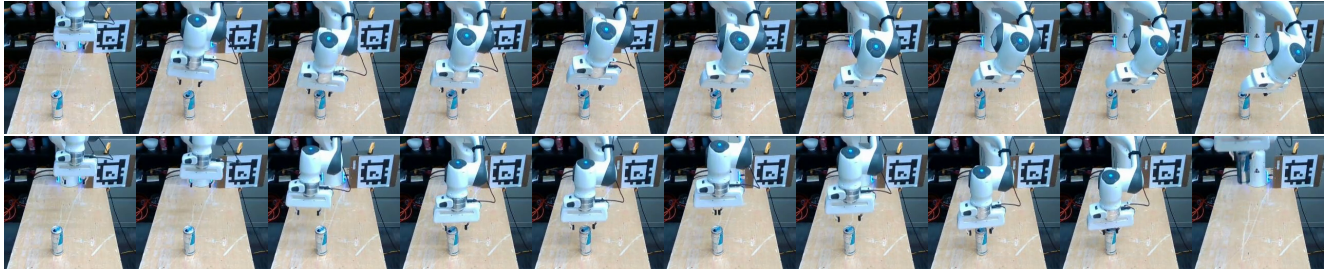


(3) Stack the Orange Cup onto the Green Cup

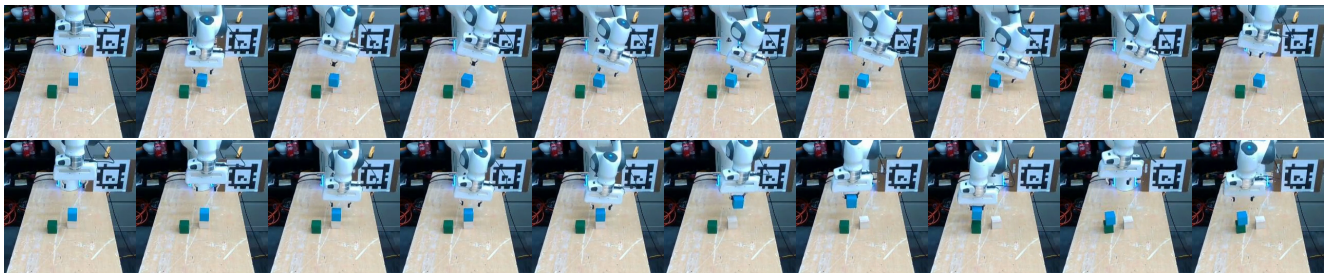


(4) Close the Laptop Lid Fully

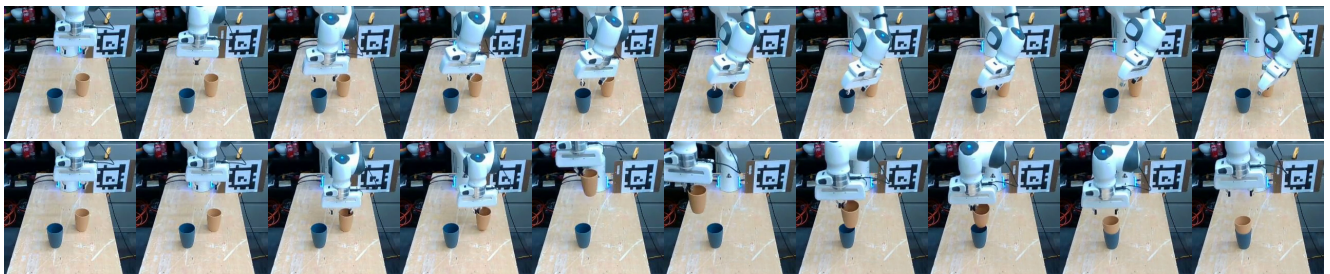
Figure 9. ID tasks: baseline (top) vs. MAPS (bottom).



(5) Grab the Red Bull Can and Lift It Up



(6) Stack the Blue Block on the Green Block



(7) Stack the Yellow Cup onto the Blue Cup



(8) Close the Laptop Lid Fully

Figure 10. OOD tasks: baseline (top) vs. MAPS (bottom).